Deep Sea Research Part II: Topical Studies in Oceanography
August 2014, Volume 106, Pages 49–67
http://dx.doi.org/10.1016/j.dsr2.2013.12.013

Effect of river runoff on sea level from in-situ measurements and numerical models in the Bay of Biscay

Irene Laiz[a,] *, Luis Ferrer[b], Theocharis A. Plomaritis[c], Guillaume Charria[d]

[a] Department of Applied Physics, Faculty of Marine Science and Environment, University of Cadiz, Campus Rio San Pedro S/N, 11510 Puerto Real, Spain
[b] AZTI-Tecnalia, Marine Research Division, Herrera Kaia, Portualdea z/g, 20110 Pasaia, Spain
[c] Department of Earth Science, Faculty of Marine Science and Environment, University of Cadiz, Campus Rio San Pedro S/N, 11510 Puerto Real, Spain
[d] DYNECO – Laboratoire de Physique Hydrodynamique et Sédimentaire, IFREMER, B.P. 70, 29280 Plouzané, France

*: Corresponding author : Irene Laiz, tel.: +34 956 956016071 ; fax: +34 956 016079 ;
email address : irene.laiz@uca.es
lferrer@azti.es ; haris.plomaritis@uca.es ; guillaume.charria@ifremer.fr

Abstract:

Daily time series of in-situ tide gauge records and river runoff data were analysed to investigate the contribution of river discharge storm events to sea level in the Bay of Biscay. Three main river systems were considered for this study, representing cases of small (Nervión, 1900 km^2), medium (Adour, 16,880 km^2) and large (Gironde, 84,811 km^2) watershed basins. Typical storms correspond to water discharge rates of 150, 700, and 1100 m^3 s^{-1} from the Nervión, Adour, and Gironde rivers, respectively. The effect of these events on daily mean sea level was evaluated using two different approaches: (1) through the analysis of time series of tide gauges placed within the river mouths; and (2) through numerical simulations using the ROMS model (Regional Ocean Modeling System). The three selected tide gauges are located at Bilbao (Spain) for the Nervión river, Boucau-Bayonne (France) for the Adour river and Port-Bloc (France) for the Gironde river. River runoff extreme events were more notable at the two tide gauges located within the largest rivers, namely, Adour and Gironde, where approximately 13% and 53.6% of the pressure-adjusted sea-level variance was explained by those events. The results obtained from the ROMS simulations suggest that the main effect of river discharge storm events occurs as a response to the input of lower salinity water. This plume of overlaying less dense water would produce a sea-level increase around the river mouth and along the coast, suggesting the generation of a coastal density current through the balance between the Coriolis force and the cross-shore pressure gradient. The main area of influence of the selected river discharges was confined to the river mouth for the Nervión, but extended up to approximately 28 km (33 km) offshore for the Adour (Gironde) river, before turning northward to flow as a density current along the coast.

Keywords : Bay of Biscay ; Sea level ; Tide gauges ; River discharge ; ROMS modelling

1. Introduction

Tide gauges are the main source of coastal sea level data, spanning from decades to more than a century back in time. As such, they provide valuable data for calculating seasonal sea level cycles and other low-frequency oscillations such as climatic signals around the globe (Lisitzin, 1974; Pattullo et al., 1955; Tsimplis and Woodworth, 1994). Tide gauge data were considered as representative of the coastal and open ocean sea level variations until the development of satellite altimetry, that highlighted discrepancies between the two signals (Marcos and Tsimplis, 2007a). Tide gauge measurements are clearly influenced by the physiographic characteristics of their geographic location (Vinogradov and Ponte, 2011). In fact, they are mainly located within major ports for historical reasons, with the aim of providing data for safe navigation. Ports can be placed in open or protected coasts or even within bays and estuaries. Hence, tide gauge signals can be influenced by standing wave generation and local resonance generated by the continental shelf and coastline conditions (Pugh, 1987). The main sources of coastal sea level variability are atmospheric pressure and wind set-up, changes in steric height due to changes in temperature and freshwater content, and mass variations related to the evaporation and precipitation cycle and to river runoff. The latter can induce important seasonal sea level fluctuations in regions located near river outflows (Tsimplis and Woodworth, 1994). As a result, sea level patterns can be rather complex in coastal areas. While the contribution of steric and meteorological effects to tidal records has been on the spotlight of research mainly due to their effect on the long term statistical properties of the records, such as sea level cycles and long-term trends, the contribution of river runoff has received less attention. Recently, Laiz et al. (2013) studied the effect of river discharges on the sea level

seasonal cycle along the coast of the Gulf of Cadiz and concluded that only the Guadalquivir river flow, with large discharge rates during storm events (> 300 $m^3 s^{-1}$) had a noticeable effect, explaining approximately 18% of the pressure-adjusted sea level variance measured at a tide gauge located at about 5.3 km from the river mouth. This effect was very small (~2%) at a neighbouring tide gauge separated 31 km in the longshore current direction, and null at the closest altimetry point, located at a distance of about 33 km offshore in the cross-shore direction. Based on these results, the authors concluded that the effect of the Guadalquivir river flow is confined within the river mouth and along a small fringe near the coast, following the extension of the river plume described in previous studies (García Lafuente et al., 2007).

In this work, the effect of river discharges on sea level measurements from selected tidal gauges situated within river estuaries along the Bay of Biscay will be addressed. More specifically, and due to the torrential character of the rivers that flow into the Bay of Biscay, we will explore the contribution of river discharge storm events on the non-tidal sea level variability. For this purpose, daily means of sea level heights from three tide gauge stations situated, respectively, within the mouth of a small (Nervión), medium (Adour) and large (Gironde) river, as well as daily river discharge rates will be analysed using a peak over threshold analysis (POT) in order to see the influence of one signal on the other. With the aim of analysing the offshore extent of such storm plume events, numerical simulations will be performed with ROMS. The above analyses, apart for offering improved sea level records, also give an insight to possible risks on the coastal environment arising from the interaction of sea level and river discharges. This work is organised as follows: Section 2 describes the data and

methodology; Section 3 introduces the model used; Section 4 discusses the obtained results; and Section 5 presents the main conclusions.

2. Study Area

The Bay of Biscay extends approximately from 43ºN to 49ºN and from 12ºW to the western French Atlantic coast (Figure 1). In this region, the continental shelf is very narrow along the Spanish coast and off the French Basque country, and widens northward along the French coastline. The bathymetry of the Bay of Biscay is constraining a complex circulation system, with spatial and temporal heterogeneity. The general circulation over the abyssal plain is mainly anticyclonic in the upper layer from ~50m to 500m (Pingree, 1993) and rather weak, with typical velocities of 1-2 cm s^{-1} in the surface layer (Pingree and Le Cann, 1989). Friocourt et al. (2007) explored its seasonal variability using a numerical ocean circulation model, obtaining a continuous flow whose position and eastward extent vary seasonally, presenting seasonal reversals. More recently, Charria et al. (2013) analysed a large dataset of Lagrangian drifter trajectories to describe the residual seasonal circulation of the surface wind mixed layer in the Bay of Biscay. Their results showed an anticyclonic circulation over the abyssal plain mainly in spring and summer that shifted south of 45.5ºN during autumn and winter. These seasonal changes respond to the wind field seasonal variations in the region (Isemer and Hasse, 1985a, b). Moreover, the general circulation over the abyssal plain is highly influenced by the slope current and the presence of mesoscale features, such as cyclonic and anticyclonic eddies, that affect the exchange between the abyssal plain and the shelf. Eddies in this region have been studied using deep-drogued and Lagrangian drifters, remotely sensed data, hydrographic observations and numerical

models (Charria et al., 2013; Ferrer and Caballero, 2011; Paillet, 1999; Pingree, 1979, 1984; Pingree and Le Cann, 1992a, b; Serpette et al., 2006; van Aken, 2002).

The circulation along the continental slope is generally weak (5-10 cm s^{-1}) and flows eastward along the North Spanish slope and poleward along the Aquitaine, Armorican and Celtic shelves, in the along-slope direction, with spatial and seasonal variations (Pingree and Le Cann, 1990; Pingree et al., 1999). Pingree et al. (1999) analysed long term Eulerian current meter data along the European continental slopes and showed a SOMA (September-October / March-April) seasonal response. The SOMA signal is also evident in mean wind and mean wind stress data in the region and is linked to the seasonal variations of the Azores high pressure cell, *AH* (Pingree and Le Cann, 1990). Consequently, the main wind direction in the Bay of Biscay shifts from southwesterly to northwesterly. In terms of the wind stress, northwesterly wind stress is dominant from spring to late summer with stronger westerly wind stress from autumn to early spring (Le Cann and Pingree, 1995). Slope currents over the northern Spanish coasts are intensified during autumn and winter when the Iberian Poleward Current (IPC) enters the Bay of Biscay (Pingree and Le Cann, 1992a), but they are subject to interannual variations (Garcia-Soto et al., 2002). This warm water extension of the IPC over the Cantabrian region usually develops around Christmas, so it has been named "Navidad" (Frouin et al., 1990; Pingree and Le Cann, 1992b). In spring, the circulation reverses showing weak equatorward currents along the Celtic and Armorican slopes, and westward along the northern Spanish coasts. The latter intensify in summer, reaching velocities of about 13.5 cm s^{-1} (Charria et al., 2013). Over the Aquitaine, Armorican, and Celtic slopes, however, the observed equatorward currents are weak during summer (1.5 cm s^{-1}). Evidence of such westward (equatorward) flows over the Bay of Biscay slopes had previously being reported (Pingree and Le Cann, 1990;

Serpette et al., 2006). This alternation of poleward and equatorward flows can promote slope-ocean exchanges, mainly in the vicinity of topographic features (Serpette et al., 2006). Previous authors studied different mechanisms that can promote shelf-slope exchange within the Bay of Biscay, such as the "Navidad" flow (Pingree and Le Cann, 1992a), the presence of anticyclonic slope eddies (SWODDIES, Pingree and Le Cann, 1992b), or the inertial overshoot triggered at promontories like spurs and canyons (Pingree et al., 1999).

Over the shelf, the circulation is mainly controlled by wind, tides, and density currents induced by river discharges (Charria et al., 2013; Ferrer et al., 2007; Fontan et al., 2006; González et al., 2004; Koutsikopoulos et al., 1998; Lazure and Jegou, 1998; Le Cann and Serpette, 2009; Pingree and Le Cann, 1989). The general circulation is weak, with residual sub-tidal currents of about 2-5 cm s^{-1}. Barotropic semidiurnal tidal currents dominate the circulation over the shelf (Le Cann, 1990; Pingree et al., 1982). Residual surface (~15-75m) currents over the north Spanish continental shelf follow the same seasonal pattern observed along the slope following the wind regime seasonal variations (Pingree and Le Cann, 1989): eastward currents are observed in autumn (5-10 cm s^{-1}); in spring, the flow starts veering westward and is fully developed in summer with large velocities that reach 13.5 cm s^{-1} (Charria et al., 2013). On the Aquitaine and Armorican shelves, a surface (from ~15 m to ~80 m depth) poleward flow is observed in autumn and winter, showing small velocities over the Aquitaine shelf (~3 cm s^{-1}) and increasing values up to 16 cm s^{-1} from about 46ºN to 48ºN (Charria et al., 2013). Previous studies had also described a surface poleward current over the Armorican shelf along the 100 m isobath with average speeds of about 10 cm s^{-1} in autumn and bursts of 20 cm s^{-1} (Lazure et al., 2008). Over the Aquitaine shelf, residual currents flow poleward in spring, with average velocities of about 5 cm s^{-1}, and equatorward during

summer, with smaller velocities of about 2 cm s^{-1} (Charria et al., 2013). In spring and summer, weak (< 3 cm s^{-1}) equatorward currents are observed along the Armorican shelf, along with a south-eastward current in the Celtic sea that enters the Armorican shelf with an average velocity of ~6 cm s^{-1} (Charria et al., 2013). On the northern Armorican Shelf, early summer winds can be west-northwest and hence, the shelf monthly mean wind driven currents will show SOMA-like seasonality. The maximum southward shelf transport wind stress response near 48° N occurs with winds from the NW (i.e. 332°T, Pingree and Le Cann, 1989). Density currents are observed in the vicinity of estuaries due to the river freshwater discharges; these induce a poleward circulation modulated by wind (Froidefond et al., 1998; Hermida et al., 1998). Hence, the offshore extension and direction of spread of the low-salinity water presents a marked wind-induced seasonal cycle (Puillat et al., 2004) with inter-annual variability (Puillat et al., 2006; Puillat et al., 2004). Lazure and Jegou (1998) analysed the behaviour of the Loire and Gironde (France) river plumes using a numerical model. Their results showed that during early winter and periods of high river discharge, plumes spread northward and alongshore with speeds of about 10 cm s^{-1}; under low river runoff and northwest wind conditions, the northward spreading of the low-salinity plumes may be stopped and driven offshore or even southward. More recently, Lazure et al. (2009) implemented the regional ocean model MARS3D (Model for Application at Regional Scale) to study the hydrology of the Bay of Biscay. The model included freshwater discharges from two major rivers (i.e., Loire and Gironde) and from 23 smaller rivers located within Brittany and the Basque Country and was able to accurately reproduce the dynamics of the main river plumes over the shelf. Ferrer et al. (2009) carried out a numerical experiment using a Lagrangian Particle-Tracking model coupled to the hydrodynamic model ROMS (Regional Ocean Modeling System) to

assess the potential connection between large river discharges and the low-salinity waters observed within the southeastern part of the Bay of Biscay over a region extending about 15-20 km offshore. For this purpose, they included freshwater discharges from the Adour (France), Nervión, Oria, Deba, Urola, Urumea, and Bidasoa (Basque Country) rivers. Their results showed that, while the low-salinity plume generated by the Adour river discharge spread northward, hence not affecting the region under study, discharges from the Nervión, Oria, Urola and Urumea rivers were the main factors contributing to the presence of the observed low-salinity water in the SE Bay of Biscay.

The two main rivers in the Bay of Biscay are the Loire and Gironde, both located at the French Atlantic coast (Figure 1). Their annual mean flow is around 900 $m^3 s^{-1}$, with large peaks in winter or spring that can exceed 3000 $m^3 s^{-1}$, and minimum values in summer. The Gironde estuary is formed from the meeting of the rivers Dordogne and Garonne and represents the largest estuary in western Europe. It presents seasonal flow rates, but is subject to strong interannual variations, showing maximum discharge rates in winter or spring, depending on the year (Bergeron, 2004). Smaller rivers, such as the Adour (Figure 1) with a mean discharge rate of about 300 $m^3 s^{-1}$ and peak flows exceeding 1000 $m^3 s^{-1}$ at short intervals during winter and spring, can also induce significant density currents (Brunet and Astin, 1999; Puillat et al., 2004). In fact, the Adour river constitutes the main source of fresh water onto the Basque (Figure 1) continental shelf (Valencia et al., 2004). Within the southeastern Bay of Biscay, the rivers are torrential in character, with very short time-lags between the precipitation and resulting river discharge (Ferrer et al., 2009). Their maximum flow rates occur principally in spring and autumn, and minimum rates at the end of summer. Major river

discharges draining this region include those of the Nervión, Oria and Bidasoa, with mean annual flows of 20-30 $m^3 s^{-1}$ (Provincial Councils of Bizkaia and Gipuzkoa).

Sea level variations in this region are mainly tidally driven, with their dynamics dominated by the barotropic semidiurnal tidal component M2 (Le Cann, 1990, Sinha and Pingree, 1997). Moreover, in the northern part of the Bay of Biscay, where the continental shelf is wider, the nonlinear generation of higher harmonics such as M4 and M6 also becomes important (Le Cann, 1990, Sinha and Pingree 1997). In terms of the sea level low frequency variability, the main forcing agents (Dussurget et al., 2009; García-Lafuente et al., 2004; Marcos and Tsimplis, 2007b) are oceanographic (steric effect) and meteorological, the latter through the inverted barometer response and wind setup. García-Lafuente et al. (2004) studied the sea level seasonal variations around Spain from tide gauge measurements, including stations located within the Bay of Biscay. At the Bay of Biscay, a well defined annual cycle was observed, with an amplitude of 5.5 cm that peaked in late September. The semiannual cycle was smaller, with an amplitude of 3.0 cm that was mainly forced by atmospheric pressure and wind setup. The annual cycle, however, did not show the same meteorological origin; rather, it seemed to be related to the steric effect. Sea level corrected by atmospheric pressure and wind peaked in October and showed a phase lag of ~2 months with the steric signal, that could be related to the hydrological cycle in the Bay of Biscay, to strong river runoffs or even to the surface circulation seasonal variations (García-Lafuente et al., 2004). The authors hypothesized that the geostrophic adjustment of the shelf currents could induce an additional sea level cycle that could shift the overall seasonal maximum toward winter. More recently, Caballero et al. (2008) studied the sea level variability in the Bay of Biscay from altimeter data, corroborating that the dominant signal was the annual cycle, also in agreement with Pingree and Garcia-Soto (2004). The altimeter-

derived annual signal (i.e., corrected from meteorological effects), presents the highest amplitudes over the slope and shelf regions (2.5-6.5 cm) and lower values in the ocean basin. The maximum values over the shelf and slope occurs in October (i.e., at the end of the heating cycle), with the exception of the northern French shelf and the northwestern Iberian Peninsula where the peak occurs in November. The authors suggest that the November maximum over the northwestern Iberian Peninsula might be related to the northwar propagation of the IPC. Over the ocean basin, tha annual cycle also peaks in October, expect for some regions where it peaks in September. Overall, the authors conclude that the annual signal is mainly due to the steric effect, as also mentioned by Pingree and Garcia-Soto (2004). Marcos and Tsimplis (2007b) used long sea level records to explore the temporal and spatial variability of the sea level seasonal signal in southern Europe, including the southern part of the Bay of Biscay. They showed that the sea level annual amplitudes and phases varied significantly with time and that this variability disminished after removing the atmospheric contribution (i.e., atmospheric pressure and wind) from the records. Finally, since tidal gauges in the Bay of Biscay are mainly located within river estuaries, they are also expected to be influenced by river discharge.

3. Data and methods

3.1 Tide gauge data

Time series of hourly sea level heights were retrieved for three tide gauge stations placed within river mouths around the Bay of Biscay (see Figure 1). The Bilbao station, located within the Nervión river mouth (43.34ºN, 3.04ºW) belongs to the Spanish Puertos del Estado Tide gauge Network (REDMAR, http://www.puertos.es/). It is an acoustic sonar measuring the sea level every 5 min with an accuracy of 2.5 mm

and a resolution of 10 mm, assuming a 5 m tidal range and a 1min integration period for the averaged measurements (Martín and Pérez, 2006). Data span from 07/01/1992 until 25/02/2011. Time series were low-pass filtered using a cosine-Lanczos filter with a 40 h half-power cut-off in order to remove tidal oscillations and near-inertial signals (Emery and Thomson, 2004), and then averaged to produce daily means. The Boucau-Bayonne and Port-Bloc stations are located on the French coast, within the Adour river mouth (43.53ºN, 1.51ºW) and the Gironde Estuary (45.57ºN, 1.06ºW), respectively. They both belong to the Service Hydrographique et Océanographique de la Marine (France). Time series were retrieved from the SONEL data assembly centre (http://www.sonel.org/). The Boucau-Bayonne tide gauge record spans from 23/05/1967 until 29/05/2011. The Port-Bloc time series covers the time period 19/04/1959 to 29/05/2011. These tide gauges were equipped with Guided Radar Level Meters (Optiflex 1300C) in 2009 (Boucau-Bayonne) and 2010 (Port-Bloc). Measurements are integrated over 10 min for the averaged measurements. Sea level measurements have a resolution of 10 mm for 95% of the provided data. The Boucau-Bayonne and Port-Bloc station data have been de-tided by the SONEL data assembly centre using a Demerliac filter with a symmetric window of 71 coefficients (Demerliac, 1974). In all cases, the sea level is measured with respect to the tide gauge zero and data are subject to standard quality control procedures by each managing authority. Prior to other computations, outliers were removed from the three time series using an iterative standard deviation filter. Finally, data were detrended using a linear robust fit. The resulting time series are referred to as *MSL*. Due to the large data gaps encountered in the tide gauge and river discharge records (see Section 2.3 below), we tried to select, for each location, the largest possible common period between the *MSL* and river discharge time series without large data gaps (i.e. gaps of less than 10 days). The resulting common full year periods were 1996-

2008 for the Bilbao-Nervión data (Bil-NV, Figure 2b), 1979-1996 and 2000-2008 for Bayonne-Adour (BY-AD, Figure 3b), and 2002-2009 for Port-Bloc-Gironde (PtB-GR, Figure 4b).

3.2 River discharge

Time series of daily discharge rates (*Q*) corresponding to the three rivers mentioned above were gathered. Data for the Nervión river were provided by the Departamento de Medio Ambiente (Diputación Foral de Bizcaia, Spain) for the time period 01/10/1995 to 30/09/2009. As for the Adour and Gironde, data were retrieved from the Banque Nationale d'Hydrométrie et d'Hydrologie (HYDRO) of Ministère de l'Environnement et du Développement Durable (France). The Adour river time series spans from 01/01/1967 to 31/12/2008. The Gironde time series, obtained as the sum of the Garonne and Dordogne rivers discharge rates, covers the period 01/01/1952 to 31/12/2010. As mentioned in Section 3.1 above, the length of each time series was reduced due to the presence of large data gaps (see Figures 2c, 3c, and 4c).

The three rivers selected represent cases of small (Nervión, 1900 km^2), medium (Adour, 16880 km^2) and large (Gironde, 84811 km^2) watershed basins. The Nervión river presented a mean discharge rate of 21 m^3 s^{-1} for the selected period, with maximum runoffs of 534 m^3 s^{-1}. The Adour river showed mean outflows of 300 m^3 s^{-1} and 254 m^3 s^{-1} for each of the selected periods, with maximum discharge rates of 2680 and 2045 m^3 s^{-1}, respectively. Finally, the mean / maximum discharge rate of the Gironde river for the time period under study was 733 m^3 s^{-1} / 6068 m^3 s^{-1}. Overall, the three rivers show the largest water discharges during autumn, winter or spring, the latter probably related to the spring thaw, and low discharge rates over the summer.

3.3 Atmospheric pressure and wind

Time series of atmospheric pressure at sea level and zonal and meridional wind components at 10 m were retrieved from the NCEP/NCAR Reanalysis 6-hourly Products (Kalnay et al., 1996) from the CISL Research Data Archive (http://rda.ucar.edu/). Data are freely available with a spatial resolution of 0.5º x 0.5º on a global grid. For the present study, three sets of time series were extracted each one corresponding to the closest grid point to each tide gauge station and spanning the time period indicated in Section 3.1. The distances to the tide gauges are approximately ~18.1 km (Bilbao), ~3.3 km (Boucau-Bayonne) and ~9.0 km (Port Bloc). Time series were filtered using a 13-point moving average filter, so that daily values on each day were computed as a 72-hour mean centred on that day in order to suppress diurnal and higher frequency changes (Barron et al., 2004) (Figures 2a, 3a and 4a). In the case of atmospheric pressure, this procedure increased the linear correlation with *MSL* from no correlation to correlation values of -0.8, -0.7, and -0.8 for the Bilbao, Boucau-Bayonne and Port-Bloc stations, respectively. Finally, wind stress components were obtained using the drag coefficient as in Large and Pond (1981).

3.4 Temperature and salinity

Time series of temperature and salinity profiles daily means were retrieved from the ROMS model simulation that included freshwater river discharge (see section 4 below for details) for the time period under study. Data were spatially averaged over the offshore part of the Bay of Biscay in order to produce a basin-wide time series of temperature and salinity profiles. These were then used to compute the contribution of the basin-wide steric height (*SH*) to the sea level variations as a combination of the

thermal expansion (SH_T) and haline contraction (SH_S) of the whole water column (Tomczak and Godfrey, 1994):

$$SH = SH_T + SH_S = -\frac{1}{\rho_0}\left[\int_{-H}^{0} \frac{d\rho}{dT} T' \, dz + \int_{-H}^{0} \frac{d\rho}{dS} S' \, dz\right] \quad (1)$$

T' and S' are the temperature and salinity deviations referenced to their climatic annual mean values; ρ is water density; ρ_0 is the sea surface density and H is the reference depth, set to 1000 m.

3.5 Statistical methods

Before addressing the effect of river discharge on sea level, a stepwise multiple regression was performed for each tide gauge in order to evaluate the percentage of sea level variability (adjusted R^2), explained by the different forcing factors considered, namely, atmospheric pressure, zonal and meridional wind stress components, steric effect, and river discharge. When performing multiple regressions, as in our case, R^2, or *coefficient of multiple determination* is an expression of the proportion of the total variability in the dependent variable (i.e., sea level) that is attributable to its dependence on all the other variables considered. A limitation on R^2 is that its value may increase even when the new variable added to the regression model does not explain much of the dependent variable. Hence, adjusted R^2 is used to compensate for this; i.e., its value will only increase when the addition of another variable adds to the explanatory power of the model. Finally, and in order to study the relationship between river discharge and sea level, two statistical methods were used, namely the Cross Wavelet Transform and the "peak-over-threshold" analysis.

The Cross Wavelet Transform (XWT) is a powerful method for estimating the relationship between two time series x_n and y_n. It is constructed from the Continuous Wavelet Transform (CWT) of each of the time series and is defined as $W^{XY} = W^X W^{Y*}$, where W^X and W^Y represent the CWT of time series x_n and y_n, respectively, and * denotes complex conjugate (Grinsted et al., 2004). The choice of the appropriate mother wavelet depends on the nature of the signals and on the type of information to be extracted from them (Torrence and Compo, 1998). Here we used the XWT method to examine linkages between river discharge rate and mean sea level at the three locations under study for the common selected time periods. More specifically, due to the episodic torrential character of the rivers, the study was focused on identifying sporadic events in frequency bands where the river discharge and mean sea level time series were occurring at the same time. For this purpose, the Paul mother wavelet was used because it is expected to provide a better temporal resolution and thus, it can identify isolated events more accurately than other wavelets (De Moortel et al., 2004). The cross wavelet power was calculated in order to estimate the covariance as a function of frequency.

In addition, a "peak-over-threshold" (POT) analysis was applied in order to obtain a relationship between the maximum Q and mean sea level values for extreme events. The POT approach consists in retaining all peak values that exceed a certain truncation threshold from a time series ensuring that they contain most of the information about extreme processes (Lang et al., 1999). When compared with other methods dealing with extreme hydrologic events, such as the "maximum flood approach", it offers the advantage of considering a wider range of extreme events (peaks) and the possibility of controlling the number of such occurrences to be included in the analysis through the appropriate selection of the threshold. The lack of a universal method for choosing the threshold value is, in fact, one of the complexities associated

with the POT approach. The threshold value affects the estimation of the return period by altering the fit parameters of the extreme value distribution (Caires and Sterl, 2005). However, in the present case where a correlation of extreme events needs to be obtained, threshold values are only related with the number of events selected. Hence, the selection criteria used in this study was based on the reduction of the scatter value of the POT data set. More specifically, the appropriate discharge threshold was selected following an iterative approach ("trial and error") where different threshold values were defined starting from the 95th quantile of the data and moving toward larger events (Caires and Sterl, 2005). In order to avoid including transitory peak events that cannot produce a significant surge, a 3-day moving average was applied to the Q time series before carrying out the POT analysis. The grouping parameters were calculated based on the Integral Time Scale of the autocorrelation function (Emery and Thomson, 2004) in order to avoid mean sea level from being pre-conditioned by previous peak events. The grouping parameters obtained were 6 days for the Nervión river, 10 days for the Adour, and 12 days for the Gironde. Consecutive peak events with calm conditions of less than the selected grouping parameter between them were considered as a single peak event. The procedure, carried out separately for each location, was as follows: (1) a POT sampling was carried out in the Q time series for a given threshold (Q_{Thrs}); (2) the sampled extreme events were adjusted to a linear regression line with the corresponding mean sea level values; (3) the resulting slope of the regression was used to correct the mean sea level values corresponding to events of $Q > Q_{Thrs}$ through linear regression; (4) the percentage of variance explained by that Q_{Thrs} was computed using equation (2) below. Those events characterized by $Q > Q_{Thrs}$ will be referred to as "extreme" or "storm" events. This procedure ensured the extraction of a statistically

independent data subsample of extreme events from the *Q* and mean sea level time series based on the daily discharge sequences (Lang et al., 1999).

The percentage of mean sea level variance explained was estimated using the following equation (Calafat et al., 2012; Sultan et al., 1995):

$$\%\ \ Variance\ \ Explained = 100\left(1 - \sigma^2_{residual} \big/ \sigma^2_{original}\right) \qquad (2)$$

where σ is the standard deviation and the subscript "original" / "residual" refers to the sea level time series before / after being corrected by the river discharge effects.

4. Numerical model

The hydrodynamic model used to determine the sea level, current, temperature, and salinity fields for the Bay of Biscay was the Regional Ocean Modeling System (ROMS). ROMS is an evolution of the S-coordinate Rutgers University Model (SCRUM), as described by Song and Haidvogel (1994). It has been expanded to include a variety of features, such as: high-order advection-schemes, accurate pressure gradient algorithms, several subgrid-scale parameterisations, atmospheric, oceanic, and benthic boundary layers, biological modules, radiation boundary conditions, and data assimilation.

Presently, ROMS is not designated in terms of a single model, but rather in a variety of versions that have been developed by different institutions. The numerical aspects of ROMS have been described in detail by Shchepetkin and McWilliams (2005). The model has been used to simulate water circulation in a variety of different regions of the world ocean, ranging from global to local scales (e.g. Haidvogel et al., 2000; Penven et al., 2001; Marchesiello et al., 2003; Di Lorenzo et al., 2004; Choi and Wilkin, 2007; and Ferrer et al., 2009).

The spatial domain for the Bay of Biscay configuration extended from 41.8ºN to 48ºN and from 10.8ºW to 0.8ºW, with a mean horizontal resolution of 6.6 km. Vertically, the water column was divided into 32 sigma-coordinate levels; these were more concentrated within the surface waters, where most of the variability occurs, which, in turn, retains high resolution for the sea surface processes. This will also ensure having a vertical resolution of about 0.3-0.6 m within the river mouths. The bathymetry used in the model was obtained through optimal interpolation of the ETOPO2 (2 minute digital Elevation TOPOgraphic model), GEBCO (General Bathymetric Chart of the Oceans), and IBCM (International Bathymetric Chart of the Mediterranean) data sets. This approach was adopted to obtain a realistic bathymetry, which was then smoothed to ensure stable and accurate simulations (Haidvogel et al., 2000). The smoothing parameter, *r*, that controls the slope of the sigma layers, is defined in the model as in Beckmann and Haidvogel (1993). The value of *r* was imposed not to exceed 0.2 (Haidvogel et al., 2000).

Surface forcing data were obtained from the NCEP/NCAR Reanalysis 6-hourly Products (Kalnay et al., 1996) for the time period 1994-2010 and consisted of air temperature and relative humidity at 2 m height, precipitation rate, short-wave and long-wave radiations, and wind components at 10 m height. Wind stress was calculated as in Section 3.3 above. The open boundary and initial conditions were obtained from the ECCO (Estimating the Circulation and the Climate of the Ocean, http://www.ecco-group.org) global data assimilation product for the same time period. Variables included sea surface elevation; temperature, salinity, and velocity profiles from the sea surface to the bottom depth; and the barotropic velocity components. Data have a spatial resolution of 1ºx1º and a temporal resolution of 10 days. In the vertical, the water column is divided into 46 depth levels with 10 m interval for the first 150 m.

Data from the OSU TOPEX/Poseidon Global Inverse Solution Version 5.0 (TPXO.5) were used as tidal forcing for the period 1994-2010. The model, developed by the Oregon State University (http://volkov.oce.orst.edu/tides/global.html), is a global model for ocean tides, which best-fits (in a least-squares sense) the Laplace Tidal Equations and along-track averaged data, from the TOPEX/Poseidon orbit cycles (Egbert et al., 1994). Tides are provided as complex amplitudes of earth-relative sea surface elevation (Shchepetkin and McWilliams, 2005) and tidal currents, in our case, for 10 primary harmonic constituents (M2, S2, N2, K2, K1, O1, P1, Q1, Mf and Mm). These tidal components are introduced into ROMS through the open boundaries using the Flather condition (Marchesiello et al., 2001). Volume is conserved automatically in the domain, whilst variations due to physical forcing (such as the tides mentioned above, and other subtidal components) are introduced through external data.

Using the aforementioned forcing and boundary conditions, three simulations covering the period 1994-2010 were carried out with ROMS. The first two simulations included the freshwater discharges from the Nervión, Adour, and Gironde rivers. River runoff is introduced as a volume of water in the continuity equation and mixing is provided by the model turbulence closure scheme and wind forcing. In our case, river discharge is introduced at one or several grid points (depending on the width of the river) through the surface 5m; the value of the coastal salinity in the immediate vicinity of the source is determined by the model mixing scheme. The only difference among the two model scenarios is that in one of them the salinity of the river flow was set to zero in order to simulate freshwater while in the other the river flow had local salinity values. Thus, one of the simulations (*R01*) will only reflect the addition of a volume of water on sea level while the other one (*R02*) will also simulate the sea level response to a buoyancy source. The third simulation was carried out without river inputs and will be

referred to as *control run*. In every case, the model was initialised from rest from January 1st 1994 and the solution quickly adjusted to the initial stratification. The level of kinetic energy increased initially following the growing eddy activity during the first two years of simulation. After this spin-up period, the eddy kinetic energy stayed particularly stable, oscillating quasiperiodically around an equilibrium value; this was approximately 34 cm^2 s^{-2} at the surface, in agreement with Ferrer et al. (2011) and approximating to conditions in nature, ~ 59 cm^2 s^{-2} for the Bay of Biscay (Pingree, 1993). The first valid simulation would therefore correspond to January 1st 1996. This method to obtain equilibrium conditions for numerical simulations with ROMS has been used in different regions of the world ocean with similar results (Marchesiello et al., 2003; Penven et al., 2005; Penven et al., 2001).

Daily maps of sea level modelled data were extracted around each of the river mouths for the three model simulations in order to evaluate the rivers' offshore influence on sea level. Maps for the Nervión river extended from 3.55ºW to 2.55ºW in longitude and from 43.14ºN to 43.87ºN in latitude for the same time period as the tide gauge records (i.e., 1996-2008). The region extracted around the Adour river covered from 2.55ºW to the coast and from 43.14ºN to 44.52ºN for the common years 1996 and 2000-2008. Finally, maps selected around the Gironde estuary extended from 2.55ºW to the coast and from 45.06ºN to 46.51ºN between 2002 and 2009. The effect of river discharges was addressed by comparing the mean sea level obtained between the *control run* and each of the two model scenarios that included river discharges. Furthermore, and in order to focus on the effect of extreme river discharge events, these events were sub-sampled separately for each river according to the corresponding Q_{Thrs} and the same comparison as above was carried out.

5. Results and discussion

5.1 Stepwise multiple regression

Results from the stepwise multiple regression (not shown) indicated that, overall, atmospheric pressure was the best predictor, explaining approximately 66%, 46% and 60% of the *MSL* variability at the Bilbao, Boucau-Bayonne, and Port Bloc tide gauges, respectively. An attempt was made to quantify the sea level response to the inverted barometer effect, obtaining that it was negligible at the daily scale, hence suggesting a dynamic response of the sea level to the movement of the atmospheric pressure field, as expected within shallow continental shelves (Pugh, 1987). This dynamic response is rarely possible to be separated from that caused by wind stress due to the dependence of wind stress on the atmospheric pressure disturbances. The remaining forcing mechanisms at the Bilbao location explained, respectively, 5% (zonal wind stress, i.e., the alongshore component); 4% (steric effect); 3% (meridional wind stress); and 1% (river discharge) of the sea level variability. In terms of the wind stress, results indicate that sea level at the Bilbao station responds mainly to the Ekman transport generated by alongshore winds. At the Boucau-Bayonne location, the second best predictor was also zonal wind stress (13%), with the meridional component only accounting for 3% of the variability and entering last in the regression. Due to the geographical location of this station, it is expected that sea level would be related to zonal wind stress, either through a direct effect, or indirectly through the generation of an alongshore eastward flowing current along the northern Spanish coast. Finally, river discharge and steric effect explained about 8% and 5% of the sea level variability, respectively. At the Port Bloc location, the second best predictor was meridional (i.e., alongshore) wind stress (13%), followed by zonal wind stress (~4%), river discharge (< 2%) and steric effect (< 1%). As in the case of Bilbao, this station is located within a

straight long coast, and hence, de-tided sea level is expected to be linked to the Ekman transport generated by alongshore winds (Csanady, 1982). Overall, the effect of river discharge seems negligible in all locations when using the full time series, suggesting that its effect on sea level might take place during specific events. In order to further analyze the potential response of sea level to river discharge, two statistical analysis were performed as described in sections 5.2 and 5.3 below. Time-lagged linear correlations carried out between river discharge and the other forcing mechanisms considered (i.e., atmospheric pressure, wind stress components and steric effect) revealed no correlation among them. Thus, river discharge can be considered as independent from the other variables and its effect can be addressed separately.

5.2 Sea level response to river discharge: tide gauge data

Although the sea level response to the inverted barometer effect was negligible, the XWT analysis was performed both between river discharge (*Q*) and *MSL* and between *Q* and sea level adjusted through the inverted barometer correction (*ASL*), obtaining that results were not significantly sensitive to the use of *MSL* or *ASL*, as expected. Thus, only results referring to *ASL* will be described for consistency with the results obtained in the POT analysis (see section 5.3 below). Figure 5 shows the cross wavelet power spectrum of *Q* and *ASL* for the Bil-NV system, displayed as a function of period and time. Colour contours represent cross wavelet power (i.e., the covariance of the two series) and vectors indicate the phase relationship between the two time series. It must be noted that the wavelet power is normalized by $1/\sigma^2$, where σ^2 is the variance and it does not have units (Torrence and Compo, 1998). The thin black line delineates the cone of influence (COI) in which edge effects cannot be ignored. In this case, the COI is defined as the area where the wavelet power due to a discontinuity at the edge

has dropped to e^{-2} of the value at the edge (Grinsted et al., 2004). Figure 5 shows a common annual cycle, as well as sporadic common events (mostly in spring and autumn months) at time scales between 64 and 128 days. A closer look to the *Q* and *ASL* time series for those months revealed that, generally, heavy river discharges occurring in autumn and spring resulted in higher sea level values, as for example during November-December 2005 (Figure 6). Other periods of time where high coherence was obtained showed cases of negligible river discharge rates and very small mean sea level values, as for example during April 1997 (Figure 7).

For the BY-AD system, due to the existence of large gaps within the two selected periods, the time series had to be further split into two (period 1976-1996) or four (period 2000-2008) segments. Overall, similar results to those of Bil-NV were obtained (see Figure 8), with an annual signal, though less clear due to the breakdown of the time series into shorter segments, and sporadic common events of high coherence. Such events were found between years 1979 and 1987 at time scales between 32 and 70 days approximately; years 1992 to 1994 (at time scales larger than 70 days), February 2000 (Figure 9) and 2001 (time scales between 32 and 64 days), October 2002 (periods around 32 days) and February 2004 (periods between 32 and 64 days). A more in-depth look to the *Q* and *ASL* time series for the above mentioned periods of time indicated that in general an increase/decrease in *Q* resulted in larger/smaller *ASL* values.

Finally, the PtB-GR *Q* and *ASL* time series were also split into two segments due to the presence of data gaps (Figure 10). As in the previous two cases, the annual signal shows high coherence. Common events occurred mainly during winter months (mostly January and February), associated with heavier river discharge rates (not shown). For example, high power was observed during January 2003, 2004, 2007, 2008 and 2009 at

time scales between 64 and 128 days. Figure 11 illustrates an event of very high river discharge and *ASL* values during January 2004; an event of smaller magnitude can also be observed during April-May.

Overall, results from the XWT analysis indicate that the effect of river discharge on sea level is principally concentrated on the annual signal; however, the phase lag at this scale does not seem to show a constant behaviour in any of the locations (see Figures 5, 8, and 10) and hence, a cause and effect relationship between *Q* and *ASL* cannot be clearly established for the annual signal. This could be related to the fact that the main mechanism driving the *ASL* annual signal is the steric effect. A more in depth study would be necessary, but it goes beyond the scope of this work. High common power is also observed during storm events linked to the river discharge seasonal cycle which is also subject to interannual variations. In these cases, the *Q* and *ASL* time series seem to be nearly in-phase, indicating a small time lag between high river discharge and high *ASL* values during those events. Therefore, a POT analysis was applied in order to obtain a relationship between the maximum *Q* and sea level values during storm events. Furthermore, the mean sea level time series were high-pass filtered using a cosine-Lanczos filter with a 185-day cut-off period in order to eliminate the seasonal cycle. Thus, only synoptic effects will be observed. Bearing in mind that the effect of river discharge on *MSL* can be addressed separately, a first attempt to carry out the POT analysis between *Q* and *MSL* was made, obtaining poor results mainly for the PtB-GR system. However, when using the pressure-adjusted sea level (*ASL*), a more clear effect of *Q* was obtained, suggesting that the effect of atmospheric pressure on sea level might be masking that of river discharge. Hence, only results referring to *ASL* will be discussed.

The threshold for the Bil-NV system was set to values above 150 $m^3 s^{-1}$, that resulted in a total of 21 storm events that represented only 1.5% of the time series length. The regression line obtained for the selected storm events (i.e., when $Q > Q_{Thrs}$) had the form $y = a \cdot x + b$, where x and y are the numerical values for the river discharge in $m^3 s^{-1}$ and mean sea level in m for those events. The fitted line had a slope $a = 6.7\times10^{-2}$ s m^{-2}, with a correlation coefficient of 0.56, significant at the 95% confidence level (Figure 12a). This regression line was used to correct the segments of the *ASL* time series corresponding to the selected storm events. The mean value of the corrected *ASL* segments (i.e., storm periods) was reduced by approximately 13.6 cm, with the river discharge explaining about 10% of the *ASL* variance during the storm events. However, when comparing the mean sea level value of the full time series for the uncorrected and corrected *ASL* (ASL_Q, hereafter), a negligible difference (~0.2 cm) was observed. Furthermore, no reduction in the ASL_Q time series variance was obtained. This seems to indicate that, although there is a good correlation between river discharge rates and *ASL* during storm events, the cumulative effect of such storms on sea level is weak, as also observed with the stepwise multiple regression. This is probably due to the fact that this river presented very few storm events (i.e., $Q > 150$ $m^3 s^{-1}$ represented only 1.5% of the time series length) and that these did not show very heavy discharge rates for the selected period. In fact, the maximum discharge rates observed during the study period were 534 $m^3 s^{-1}$, with an average of 225 $m^3 s^{-1}$ during the extreme events.

Since the POT method is not affected by the presence of large gaps in the time series, the two periods selected for the BY-AD system (1976-1996 and 2000-2008) were jointly used. In this case, Q_{Thrs} was set to 700 $m^3 s^{-1}$. A total of 113 storm events were found that produced a linear fit of the type $y = a \cdot x + b$, as before, with a slope $a = 1.3\times10^{-5}$ s m^{-2}, and a correlation coefficient of 0.51, significant at the 95% confidence

level (Figure 12b). When correcting the segments of the *ASL* time series corresponding to the storm events (i.e., when $Q > Q_{Thrs}$) using the linear regression line obtained, its mean value was reduced by approximately 15.6 cm for the events and in about 1.1 cm for the full period. River discharge explained approximately 13% of the *ASL* variance during the storm periods and about 4% of the full *ASL* time series variance.

Due to the large size of the Gironde river catchment, the threshold value for the PtB-GR system was set to 1100 $m^3 s^{-1}$. Moreover, the selected extreme events adjusted to a power function of the form $y = a \cdot x^b$, where x and y are the numerical values for the river discharge in $m^3 s^{-1}$ and mean sea level in m for those events. The coefficients obtained were a = 0.229 s m^{-2} and b=0.050 (dimensionless) with a correlation coefficient of 0.75 significant at the 95% confidence level (Figure 12c). When correcting the *MSL* time series using the resulting power function, a sea level reduction of approximately 3 cm was obtained during the selected events. The percentage of *ASL* variance explained by river discharge during the selected storm events was approximately 53.6%.

Overall, the POT results suggested that although the effect of *Q* on *MSL* could be addressed separately because it is independent from the other forcing mechanisms considered, their effect on *MSL* can be actually masking that of *Q*. The main forcing factors were atmospheric pressure and wind stress, the former producing a dynamic response on the sea level that is very difficult to separate from that caused by wind stress. Pascual et al. (2008) suggested that the best method to remove meteorologically induced signals from tide gauge sea level records was using the residuals computed by the HAMSOM model within the European Union project Hindcast of Dynamic Processes of the Ocean and Coastal Areas of Europe (HIPOCAS) (Guedes Soares et al., 2002; Sotillo et al., 2005). This model computes the response of sea level from the

equations of motion instead of assuming an empirical formulae to correct the wind set-up and an isostatic inverted barometer response. However, the HIPOCAS hindcast data were produced for the years 1958-2001, hence not covering the full time period analyzed in this study. Thus, a first attempt to eliminate the masking effects of atmospheric pressure on *MSL* was done by simply adjusting the *MSL* time series through the inverted barometer correction. When carrying out the POT analysis between *Q* and *ASL*, results indicated that extreme river discharge values resulted in higher *ASL* values at the three tide gauge records. In these cases, correcting the *ASL* values using linear (Nervión, Adour) or power (Gironde) functions, as explained in Section 3.4, produced *ASL* values similar to those observed along the *ASL* time series during non-storm conditions. However, some extreme runoffs were accompanied by lower sea level (*ASL*) values, probably related to the atmospheric pressure (dynamic response) or wind stress fields. In those cases, the *ASL* values obtained after correcting with the above mentioned functions were too low when compared to those observed before such events. Addressing the effect of other forcing mechanisms, such as wind set up, would help to elucidate those anomalously low *ASL* values observed during high river discharge events.

5.3 Sea level response to river discharge: numerical model

Figure 13 shows the ROMS model results for the region surrounding the Nervión river. Maps are calculated by subtracting, on a point-by-point basis, the average mean sea level of the two model simulations that are being compared: (a) simulation with rivers (*R01*) versus *control run* for the full time period; (b) simulation with rivers and zero salinity (*R02*) versus *control run* for the full time period; (c) and (d) are equivalent to (a) and (b) but only for extreme events. The *R01* model simulation showed

an average mean sea level very similar to that of the *control run*, both when looking at the full time period (panel a, sea level differences < 0.1 cm) and when focusing on the storm events (panel c, sea level differences < 0.5 cm). Thus, the addition of a relatively small volume of water (i.e., a mean / maximum discharge rate of 21.3 $m^3 s^{-1}$ / 534 $m^3 s^{-1}$) with the same salinity (i.e., density) as the surrounding waters does not produce any significant effect. The *R02* model simulation shows an average sea level increase of approximately 0.7 cm at the discharge point for the full time period (panel b) that quickly decreased to about 0.3 cm at a distance of 25 km from the discharge location. When looking at the storm events (panel d), a mean sea level difference of about 2 cm is observed at the discharge point, very similar to that obtained at the Bilbao tide gauge. In this case, the buoyancy plume extends further offshore up to a distance of about 30 km from the discharge point, where it shows a mean sea level difference of about 0.3 cm. The extension of the buoyancy plume does not seem to form a permanent coastal current over the full studied period; rather, it appears during storm events. Similarly, previous studies (Ferrer et al., 2009) had shown that the freshwater input from the Nervión river can generate low-salinity plumes that are observed under specific oceanic-meteorological conditions and that extend over 15-20 km from the river mouth.

Figure 14 shows the ROMS model results for the region surrounding the Adour river. Maps are calculated as above. The *R01* simulation showed no differences with the *control run* for the full time period (panel a) and presented an average mean sea level increase of just 0.15 cm at the discharge location for the extreme events (panel b). No more differences were observed beyond the river mouth, again suggesting the immediate mixing with the surrounding waters. When imposing a zero salinity value for the river runoff (simulation *R02*), sea level at the discharge location increases an average of about 3 cm for the full time period (panel b) and about 6 cm during the storm

events (panel d). In both cases, a plume of higher mean sea level is observed spreading offshore from the river mouth up to approximately 28 km (measured perpendicular to the coast), where it shows a maximum difference of 0.5 cm. The extension of this plume presents similar values to those reported by Ferrer et al. (2009) for the same river. This plume then extends northward along the coast, suggesting the generation of a coastal density current through the balance between the Coriolis force and the cross-shore pressure gradient developed due to the "freshening" of coastal waters (McClimans, 1986). The difference in sea level at the discharge point obtained from the POT analysis (~15.6 cm) and the ROMS *R02* simulation (~6 cm) for the storm periods is probably due to the time period difference. In fact, Figure 3c shows that the largest river discharge events took place during years 1981, 1982, 1993 and 1992, not included in the ROMS results.

The Gironde river results are shown in Figure 15. The *R01* simulation showed maximum sea level differences with respect to the *control run* of about 0.4-0.6 cm at the discharge location. A small plume of sea level differences of about 0.2 cm at the front extends around 33 km offshore, both for the full time series (panel a) and for the storm events (panel c). Note that this plume is not visible due to the figure's contour scale. This reflects the size of the mean / maximum discharge rates (733.2 $m^3 s^{-1}$ / 6068 $m^3 s^{-1}$) of this river that continuously adds a large volume of water to the coastal area. However, since the added water has the same density as the surrounding waters, it does not form a density current. When imposing the river outflow with zero salinity (model run *R02*), an average increase in sea level (with respect to the *control run*) of 5 cm / 7 cm was observed at the river mouth for the full time series / extreme events. Moreover, a plume of higher sea level extended offshore, more notably for the selected extreme events (panel d). For the extreme events, sea level values of about 2 cm were observed

at the front of the plume, approximately 33 km distance from the river mouth, when it turned northward, again suggesting the development of a density current. The front of sea level values around 2 cm was observed up to a distance of about 105 km northward of the river mouth, consistent with the large buoyancy plumes described for this river.

6. Summary and conclusions

In this manuscript, we explored the contribution of river discharge storm events on the non-tidal sea level variability within the Bay of Biscay. For this purpose, we analysed time series of daily means of sea level heights from three tide gauge stations located within the mouth of a small (Nervión), medium (Adour) and large (Gironde) river, as well as daily river discharge rates (Q) for each of the above mentioned rivers. Moreover, we carried out three numerical simulations using the high resolution hydrodynamics model ROMS. First, a *control run* was performed that did not include river runoff. Second, a scenario including daily river discharges for each of the three rivers was carried out with the aim of simulating the effects of adding extra volumes of water to the system. Finally, a simulation including river discharges with zero salinity was performed in order to explore the effects that the low-salinity plume might have on the sea level.

Before addressing the effect of river discharge on sea level, a stepwise multiple regression was carried out for each tide gauge in order to evaluate the percentage of sea level variability (adjusted R^2) explained by atmospheric pressure, zonal and meridional wind stress components, steric effect, and river discharge. Results indicated that the best predictor was atmospheric pressure, that explained the major part of the sea level variability. The second best predictor was the alongshore wind stress component. The Bilbao and Port Bloc stations are placed within a straight long coast, and hence, de-

tided sea level is expected to respond to the Ekman transport generated by alongshore winds (Csanady, 1982). The Boucau-Bayonne station is located in a corner formed by the Spanish and French coastlines. Thus, it is expected that sea level would be related to zonal wind stress, either through a direct effect, or indirectly through the generation of an alongshore eastward flowing current along the northern Spanish coast. Sea level seemed to mainly respond dynamically to the atmospheric pressure field, as expected within shallow continental shelves (Pugh, 1987). This dynamic response is very difficult to separate from that caused by wind stress and hence, they should be jointly studied using numerical models like HAMSOM (Pascual et al., 2008). Since the available data derived for this model does not cover the time period analyzed in this study, the effect of atmospheric pressure (dynamic response) and wind stress will not be removed. Finally, time-lagged linear correlations carried out between river discharge and the other forcing mechanisms considered indicated that river discharge can be considered as independent and hence its effect on sea level can be studied separately. For this purpose, two statistical methods were used, namely the Cross Wavelet Transform and the "peak-over-threshold" analysis. Although the inverted barometer correction produced a small effect on the *MSL*, results from the POT analysis suggested that atmospheric pressure could be masking the effects of river discharge on sea level. Hence, the results presented will only refer to the sea level time series corrected with the inverted barometer (*ASL*).

Cross Wavelet Transform (XWT) analysis performed between river discharge and the pressure-corrected sea level time series (*ASL*) resulted in similar results for the three rivers; more specifically, it showed that the effect of river discharge on *ASL* is mainly concentrated on the annual signal. Since the phase lag at this scale did not seem to show a constant behaviour in any of the locations, a cause and effect relationship between *Q* and *ASL* could not be established for the annual signal. This could be related

to the fact that the main mechanism driving the *ASL* annual signal is the steric effect. A more in depth analysis would be necessary, probably using the "Morlet" mother wavelet that specifically designed to study periodic signals, but it goes beyond the scope of this work. High common power was also observed during storm events linked to the rivers seasonal cycle. In these cases, the *Q* and *ASL* time series were nearly in-phase, indicating a small time lag between high river discharge and high *ASL* values during those events. Thus, a "peak-over-threshold" (POT) analysis was carried out with the aim of obtaining a relationship between the maximum *Q* and *ASL* values during storm events. These were defined in terms of the river discharge rate exceeding a certain threshold as obtained from the POT analysis. Results from the Bil-NV system that represents the case of a small river, showed that the effect of storm events ($Q > 150$ m^3 s^{-1}) on *ASL* was mainly noticed during such events but did not propagate along the full time series, reflecting the relatively few storm events that took place during the studied period, as well as the low discharge rates observed during such events in comparison with larger rivers. This agreed with the ROMS model results that also showed a very small sea level difference confined in a small area around the river mouth, more notable during the storm events. The river runoff threshold for the BY-AD system was set to 700 m^3 s^{-1}. When correcting the segments of the *ASL* time series corresponding to the storm events, its mean value was reduced by approximately 15.6 cm for the events and in about 1.1 cm for the full *ASL* time series, with the river discharge explained approximately 13% / 4% of the *ASL* variance for the storm / full period. The ROMS simulation when zero salinity for the river outflow was imposed (simulation *R02*) indicated a maximum sea level increase of about 6 cm / 3 cm for the storm / full period. This difference is probably due to the fact that the POT analysis was performed for a longer time period that presented very large and numerous storm events. The model *R02*

simulation showed a plume of higher sea level seaward of the river mouth and along the coast, suggesting the generation of a coastal density current through the balance between the Coriolis force and the cross-shore pressure gradient. The offshore extension of this plume was approximately 28 km, in agreement with previous results for the region (Ferrer et al., 2009). Due to the large size of the Gironde river catchment, the threshold value for the PtB-GR system was set to 1100 $m^3 s^{-1}$ during the POT analysis. In this case, storm events increased the *ASL* mean value by approximately 3 cm and accounted for approximately 53.6% of the *ASL* variance during the events. The results from the numerical experiments also showed a larger sea level increase when imposing a zero salinity condition on the river outflow (simulation *R02*), corroborating the idea that an input of lower salinity (i.e., less dense) water will produce a sea level increase due to the buoyancy plume. This model simulation showed an average increase in sea level (with respect to the *control run*) of 5 cm / 7 cm at the river mouth for the full time series / extreme events. Furthermore, a plume of higher sea level extended offshore, more notably for the selected extreme events, when average sea level values of about 2 cm were observed at the front of the plume, approximately 33 km distance from the river mouth; then, the plume turned northward showing sea level values of 2 cm up to a distance of about 105 km from the river mouth, consistent with the development of a large buoyancy plume as previously described for this river.

Acknowledgements

Dr. Laiz was supported by the Ministerio de Ciencia e Innovación (Spain) through project "CLI-CGL2008-04736". Dr. Plomaritis was supported by the EU FP7 Environment Research Programme through project "MICORE" (project number 202798). We thank the tide gauge observation reference networks (French designation REFMAR) and the SONEL data assembly centre for providing tide gauge data at Port-Bloc and Boucau-Bayonne as well as Puertos del Estado (Spain) for providing the Bilbao tide gauge data. The Diputación Foral de Bizcaia (Spain) and the Banque Nationale d'Hydrométrie et d'Hydrologie (France) are also acknowledged for making available the river discharge rates.

References

Barron, C.N., Birol Kara, A., Hurlburt, H.E., Rowley, C., Smedstad, L.F., 2004. Sea Surface Height Predictions from the Global Navy Coastal Ocean Model during 1998–2001. Journal of Atmospheric and Oceanic Technology 21, 1876-1893, doi: 10.1175/jtech-1680.1.

Beckmann, A., Haidvogel, D.B., 1993. Numerical Simulation of Flow around a Tall Isolated Seamount. Part I: Problem Formulation and Model Accuracy. Journal of Physical Oceanography 23, 1736-1753, doi: 10.1175/1520-0485(1993)023<1736:nsofaa>2.0.co;2.

Bergeron, J.-P., 2004. Contrasting years in the Gironde estuary (Bay of Biscay, NE Atlantic) springtime outflow and consequences for zooplankton pyruvate kinase activity and the nutritional condition of anchovy larvae: an early view. Ices Journal of Marine Science 61, 928-932, doi: 10.1016/j.icesjms.2004.06.019.

Brunet, R.C., Astin, K.B., 1999. Spatio-temporal variation in some physical and chemical parameters over a 25-year period in the catchment of the river Adour. Journal of Hydrology 220, 209-221, doi: 10.1016/s0022-1694(99)00072-4.

Caires, S., Sterl, A., 2005. 100-Year Return Value Estimates for Ocean Wind Speed and Significant Wave Height from the ERA-40 Data. Journal of Climate 18, 1032-1048, doi: 10.1175/jcli-3312.1.

Charria, G., Lazure, P., Le Cann, B., Serpette, A., Reverdin, G., Louazel, S., Batifoulier, F., Dumas, F., Pichon, A., Morel, Y., 2013. Surface layer circulation derived from Lagrangian drifters in the Bay of Biscay. Journal of Marine Systems 109–110, Supplement, S60-S76, doi:10.1016/j.jmarsys.2011.09.015.

Choi, B.-J., Wilkin, J.L., 2007. The effect of wind on the dispersal of the Hudson River plume. Journal of Physical Oceanography, 37 (7), 1878-1897, doi: 10.1175/jpo3081.1.

Conkright, M.E., Locarnini, R.A., Garcia, H.E., O'Brien, T.D., Boyer, T.P., Stephens, C., Antonov, J.I., 2002. World Ocean Atlas 2001: Objective Analyses, Data Statistics, and Figures, CD-ROM Documentation. National Oceanographic Data Center, Silver Spring, MD, 17pp.

Csanady, G.T., 1982. Circulation in the coastal ocean. D. Reidel Publishing Company Ed., The Netherlands, 279 pp, ISBN 90-277-1400-2.

Da Silva, A.M., Young, C.C., Levitus, S., 1994. Atlas of surface marine data 1994, Vol. 1: algorithms and procedures. NOAA Atlas NESDIS 6, U.S. Department of Commerce, NOAA, NESDIS, 74pp.

Demerliac, M. A., 1974. Calcul du niveau moyen journalier. Annales Hydrographiques du SHOM. 5ème série, 2, 49-57.

De Moortel, I., Munday, S.A., Hood, A.W., 2004. Wavelet analysis: The effect of varying basic wavelet parameters. Solar Physics 222, 203-228, doi: 10.1023/B:SOLA.0000043578.01201.2d.

Di Lorenzo, E., Miller, A.J., Neilson, D.J., Cornuelle, B.D., Moisan, J.R., 2004. Modelling observed California current mesoscale eddies and the ecosystem response. International Journal of Remote Sensing, 25 (7-8), 1307-1312, doi: 10.1080/01431160310001592229.

Dussurget, R., Birol, F., Morrow, R., 2009. Investigating Bay of Biscay mesoscale and coastal ocean dynamics from satellite observations, Proceedings of the OceanObs'09: Sustained Ocean Observations and Information for Society Conference, Venice-Lido, Italy.

Egbert, G.D., Bennett, A.F., Foreman, M.G.G., 1994. Topex/Poseidon Tides estimated using a Global Inverse Model. Journal of Geophysical Research, 99 (C12), 24821-24852, doi: 10.1029/94jc01894.

Emery, W.J., Thomson, R.E., 2004. Data Analysis Methods in Physical Oceanography, Second and Revised Edition ed. Elsevier B.V, 638pp.

Ferrer, L., Caballero, A., 2011. Eddies in the Bay of Biscay: A numerical approximation. Journal of Marine Systems 87, 133-144, doi: 10.1016/j.jmarsys.2011.03.008.

Ferrer, L., Fontán, A., Chust, G., Mader, J., González, M., Valencia, V., Uriarte, Ad., Collins, M.B., 2009. Low salinity plumes in the oceanic region of the Basque Country. Continental Shelf Research, 29 (8), 970-984, doi: 10.1016/j.csr.2008.12.014.

Ferrer, L., González, M., Valencia, V., Mader, J., Fontán, A., Uriarte, A., Caballero, A., 2007. Operational coastal systems in the Basque country region: Modelling and observations. Proceedings of the Seventeenth International Offshore and Polar Engineering Conference, ISOPE, Chung, J.S., Kashiwagi, M., Losada, I.J. & Chien, L.-K. (Eds.), 1-7 July 2007, Lisbon, Portugal, pp. 1736-1743..

Fontán, A., Mader, J., González, M., Uriarte, Ad., Gyssels, P., Collins, M., 2006. Marine hydrodynamics between San Sebastián and Hondarribia (Guipúzcoa, northern Spain): field measurements and numerical modelling. Scientia Marina, 70S1, June 2006, Barcelona, Spain, 51-63.

Friocourt, Y., Levier, B., Speich, S., Blanke, B., Drijfhout, S.S., 2007. A regional numerical ocean model of the circulation in the Bay of Biscay. Journal of Geophysical Research: Oceans 112, C09008, doi: 10.1029/2006jc003935.

Froidefond, J.M., Jegou, A.M., Hermida, J., Lazure, P., Castaing, P., 1998. Variability of the Gironde turbid plume by remote sensing. Effects of climatic factors. Oceanologica Acta 21, 191-207, doi: 10.1016/s0399-1784(98)80008-x.

Frouin, R., Fiúza, A.F.G., Ambar, I., Boyd, T.J., 1990. Observations of a poleward surface current off the coasts of Portugal and Spain during winter. Journal of Geophysical Research: Oceans 95, 679-691, doi: 10.1029/JC095iC01p00679.

García Lafuente, J., Sánchez Román, A., Díaz del Río, G., Sannino, G., Sánchez Garrido, J.C., 2007. Recent observations of seasonal variability of the Mediterranean outflow in the Strait of Gibraltar. Journal of Geophysical Research 112, C10005, doi: 10.1029/2006jc003992.

García-Lafuente, J., Del Río, J., Alvarez Fanjul, E., Gomis, D., Delgado, J., 2004. Some aspects of the seasonal sea level variations around Spain. Journal of Geophysical Research 109, C09008, doi: 10.1029/2003jc002070.

Garcia-Soto, C., Pingree, R.D., Valdés, L., 2002. Navidad development in the southern Bay of Biscay: Climate change and swoddy structure from remote sensing and in situ measurements. Journal of Geophysical Research 107, C83118, doi: 10.1029/2001jc001012.

González, M., Uriarte, Ad., Fontán, A., Mader, J., Gyssels, P., 2004. Marine dynamics. In: Borja, A. & Collins, M. (Eds.), Oceanography and Marine Environment of the Basque Country, Elsevier Oceanography Series, 70, 133-157.

Grinsted, A., Moore, J.C., Jevrejeva, S., 2004. Application of the cross wavelet transform and wavelet coherence to geophysical time series. Nonlinear Processes in Geophysics 11, 561-566, doi:10.5194/npg-11-561-2004.

Guedes Soares, C., Carretero Albiach, J.C., Weisse, R., Alvarez-Fanjul, E., 2002. A 40 years hindcast of wind, sea level and waves in European waters, in: Engineers, A.S.o.M. (Ed.), 21st International Conference on Offshore Mechanics and Arctic Engineering. American Society of Mechanical Engineers, Oslo, pp. 1-7.

Haidvogel, D.B., Arango, H.G., Hedstrom, K., Beckmann, A., Malanotte-Rizzoli, P., Shchepetkin, A.F., 2000. Model evaluation experiments in the North Atlantic Basin: simulations in nonlinear terrain-following coordinates. Dynamics of Atmospheres and Oceans 32, 239-281, doi: 10.1016/S0377-0265(00)00049-X.

Hermida, J., Lazure, P., Froidefond, J.M., Jegou, A.M., Castaing, P., 1998. Seaward dispersion of Gironde estuarine waters on to Aquitanian continental shelf from hydrological, satellite and numeric data. Oceanologica Acta 21, 209-221, doi: 10.1016/s0399-1784(98)80009-1.

Huthnance, J.M., Van Aken, H.M., White, M., Barton, E.D., Le Cann, B., Coelho, E.F., Alvarez Fanjul, E., Miller, P., Vitorino, J., 2002. Ocean margin exchange—water flux estimates. Journal of Marine Systems 32, 107-137, doi: 10.1016/S0924-7963(02)00034-9.

Isemer, H.J., Hasse, L., 1985a. The Bunker Climate Atlas of the North Atlantic Ocean, Vol. 1. Springer, Berlin, 218pp.

Isemer, H.J., Hasse, L., 1985b. The Bunker Climate Atlas of the North Atlantic Ocean, Vol. 2. Springer, Berlin, 252pp.

Kalnay, E., Kanamitsu, M., Kistler, R., Collins, W., Deaven, D., Gandin, L., Iredell, M., Saha, S., White, G., Woollen, J., Zhu, Y., Chelliah, M., Ebisuzaki, W., Higgins, W., Janowiak, J., Mo, K.C., Ropelewski, C., Wang, J., Leetmaa, A., Reynolds, R., Jenne, R., Joseph, D., 1996. The NCEP/NCAR 40-year reanalysis project. Bulletin of the American Meteorological Society 77, 437-471.

Koutsikopoulos, C., Le Cann, B., 1996. Physical processes and hydrological structures related to the Bay of Biscay anchovy. Scientia Marina, 60 (Supl. 2), 9-19.

Koutsikopoulos, C., Beillois, P., Leroy, C., Taillefer, F., 1998. Temporal trends and spatial structures of the sea surface temperature in the Bay of Biscay. Oceanologica Acta 21, 335-344, doi: 10.1016/S0399-1784(98)80020-0.

Laiz, I., Gómez-Enri, J., Tejedor, B., Aboitiz, A., Villares, P., 2011. Estimation of the seasonal sea level variations in the Gulf of Cadiz (SW Iberian Peninsula) from in-situ measurements, satellite altimetry and numerical models, in: Bostater, C.R., Mertikas, S.P., Neyt, X., Velez-Reyes, M. (Eds.), Remote Sensing of the Ocean, Sea Ice, Coastal Waters, and Large Water Regions 2011. SPIE, Prague, pp. 81750K-81751 - 81750K-81712.

Laiz, I., Gómez-Enri, J., Tejedor, B., Aboitiz, A., Villares, P., 2013. Seasonal sea level variations in the gulf of Cadiz continental shelf from in-situ measurements and satellite altimetry. Continental Shelf Research 53, 77-88, doi: 10.1016/j.csr.2012.12.008

Lang, M., Ouarda, T.B.M.J., Bobée, B., 1999. Towards operational guidelines for over-threshold modeling. Journal of Hydrology 225, 103-117, doi: 10.1016/s0022-1694(99)00167-5.

Lazure, P., Garnier, V., Dumas, F., Herry, C., Chifflet, M., 2009. Development of a hydrodynamic model of the Bay of Biscay. Validation of hydrology. Continental Shelf Research 29, 985-997, doi: 10.1016/j.csr.2008.12.017.

Lazure, P., Dumas, F., Vrignaud, C., 2008. Circulation on the Armorican shelf (Bay of Biscay) in autumn. Journal of Marine Systems 72, 218-237, doi: 10.1016/j.jmarsys.2007.09.011.

Lazure, P., and A.-M. Jegou, 1998. 3D modelling of seasonal evolution of Loire and Gironde plumes on Biscay Bay continental shelf. Oceanologica Acta, 21(2), 165-177, doi: 10.1016/S0399-1784(98)80006-6.

Large, W.G., Pond, S., 1981. Open ocean momentum flux measurements in moderate to strong winds. Journal of Physical Oceanography 11, 324-336.

Le Cann, B., 1990. Barotropic tidal dynamics of the Bay of Biscay shelf: observations, numerical modelling and physical interpretation. Continental Shelf Research 10, 723-758, doi: 10.1016/0278-4343(90)90008-a.

Le Cann, B., and R. Pingree, 1995. Circulation dans le Golfe de Gascogne: une revue des travaux récents, in Acta del IV Coloquio Internacional sobre Oceanografía del Golfo de Vizcaya, 217-234.

Le Cann, B., Serpette, A., 2009. Intense warm and saline upper ocean inflow in the southern Bay of Biscay in autumn–winter 2006–2007. Continental Shelf Research 29, 1014-1025, doi: 10.1016/j.csr.2008.11.015.

Lisitzin, E., 1974. Sea-Level Changes. Elsevier Scientific Publishing Company.

Marcos, M., Tsimplis, M.N., 2007a. Forcing of coastal sea level rise patterns in the North Atlantic and the Mediterranean Sea. Geophysical Research Letters 34, L18604, doi: 10.1029/2007gl030641.

Marcos, M., Tsimplis, M.N., 2007b. Variations of the seasonal sea level cycle in southern Europe. Journal of Geophysical Research, 112, C12011, doi: 10.1029/2006jc004049.

Marchesiello, P., McWilliams, J.C., Shchepetkin, A., 2001. Open boundary conditions for long-term integrations of regional oceanic models. Ocean Modelling, 3 (1), 1-20, doi: 10.1016/s1463-5003(00)00013-5.

Marchesiello, P., McWilliams, J.C., Shchepetkin, A., 2003. Equilibrium structure and dynamics of the California current system. Journal of Physical Oceanography, 33 (4), 753-783, doi: 10.1175/1520-0485(2003)33<753:esadot>2.0.co;2.

Martín, B., Pérez, B., 2006. Assessment of accuracy and operational properties of different tide gauge sensors. WP4. Deliverable D4.1. European Sea Level Service Research and Infrastructure (http://www.puertos.es/sites/default/files/pdfs/1162197987031.pdf).

McClimans, T.A., 1986. Estuarine fronts and river plumes. In Physical Processes in Estuaries. J. Dronkers and W. van Leussen (Eds.), pp. 55-69, Springer-Verlag, New York.

Paillet, J., 1999. Central Water Vortices of the Eastern North Atlantic. Journal of Physical Oceanography 29, 2487-2503, doi: 10.1175/1520-0485(1999)029<2487:cwvote>2.0.co;2.

Pascual, A., Marcos, M., Gomis, D., 2008. Comparing the sea level response to pressure and wind forcing of two barotropic models: Validation with tide gauge and altimetry data. Journal of Geophysical Research 113, C07011, doi: 10.1029/2007jc004459.

Pattullo, J., Munk, W., Revelle, R., Strong, E., 1955. The seasonal oscillation in sea level. Journal of Marine Research 14, 88-155.

Penven, P., Echevin, V., Pasapera, J., Colas, F., Tam, J., 2005. Average circulation, seasonal cycle, and mesoscale dynamics of the Peru Current System: A modeling approach. Journal of Geophysical Research: Oceans 110, C10021, doi: 10.1029/2005jc002945.

Penven, P., Lutjeharms, J.R.E., Marchesiello, P., Roy, C., Weeks, S.J., 2001. Generation of cyclonic eddies by the Agulhas current in the lee of the Agulhas bank. Geophysical Research Letters, 27 (6), 1055-1058, doi: 10.1029/2000gl011760.

Pingree, R.D., 1979. Baroclinic eddies bordering the Celtic Sea in late summer. Journal of the Marine Biological Association of the United Kingdom 59, 689-703, doi:10.1017/S0025315400045677.

Pingree, R.D., 1984. Some Applications of Remote Sensing to Studies in the Bay of Biscay, Celtic Sea and English Channel .Remote Sensing of Shelf Seas Hydrodynamics. Elsevier Oceanography Series, 38, 287-315, doi: 10.1016/S0422-9894(08)70617-2.

Pingree R.D., 1993. Flow of surface waters to the west of the British Isles and in the Bay of Biscay. Deep-Sea Research II, 40, 369-388, doi: 10.1016/0967-0645(93)90022-F.

Pingree R.D. and B. Le Cann, 1989. Celtic and Armorican slope and shelf residual currents. Progress in Oceanography 23, 303-338, doi: 10.1016/0079-6611(89)90003-7.

Pingree R.D. and B. Le Cann, 1990. Structure, strength and seasonality of the slope currents in the Bay of Biscay region. Journal of the Marine Biological Association of the United Kingdom 70, 857-885, doi:10.1017/S0025315400059117.

Pingree R.D. and B. Le Cann, 1992a. Anticyclonic eddy X91 in the southern Bay of Biscay, May 1991 to February 1992. Journal of Geophysical Research, 97, 14353-14367, doi: 10.1029/92jc01181.

Pingree R.D. and B. Le Cann, 1992b. Three anticyclonic Slope Water Oceanic eDDIES (SWODDIES) in the Southern Bay of Biscay in 1990. Deep-Sea Research, 39, 1147-1175, doi: 10.1016/0198-0149(92)90062-X.

Pingree, R.D., Mardell, G.T., Holligan, P.M., Griffiths, D.K., Smithers, J., 1982. Celtic Sea and Armorican current structure and the vertical distributions of temperature and chlorophyll. Continental Shelf Research 1, 99-116, doi: 10.1016/0278-4343(82)90033-4.

Pingree, R.D., Sinha, B., Griffiths, C.R., 1999. Seasonality of the European slope current (Goban Spur) and ocean margin exchange. Continental Shelf Research 19, 929-975, doi: 10.1016/S0278-4343(98)00116-2.

Pingree, R., Garcia-Soto, C., 2004. Annual westward propagating anomalies near 26°N and eddy generation south of the Canary Islands: remote sensing (altimeter/SeaWiFS) and in situ measurement. Journal of the Marine Biological Association of the United Kingdom 84, 1105-1115, doi: 10.1017/S0025315404010549h.

Pugh, D.T., 1987. Tides, surges and mean sea-level: a handbook for engineers and scientists. Wiley, Chichester, 472pp.

Puillat, I., Lazure, P., Jegou, A.M., Lampert, L., Miller, P., 2006. Mesoscale hydrological variability induced by northwesterly wind on the French continental shelf of the Bay of Biscay. Scientia Marina 70, 15-26.

Puillat, I., Lazure, P., Jégou, A.M., Lampert, L., Miller, P.I., 2004. Hydrographical variability on the French continental shelf in the Bay of Biscay, during the 1990s. Continental Shelf Research 24 (10), 1143-1163, doi: 10.1016/j.csr.2004.02.008.

Serpette, A., Le Cann, B., Colas, F., 2006. Lagrangian circulation of the North Atlantic Central Water over the abyssal plain and continental slopes of the Bay of Biscay: description of selected mesoscale features. Scientia Marina 70, 27-42.

Shchepetkin, A.F., McWilliams, J.C., 2005. The regional oceanic modeling system (ROMS): a split-explicit, free-surface, topography-following-coordinate oceanic model. Ocean Model., 9, 347-404, doi: 10.1016/j.ocemod.2004.08.002.

Sinha, B., Pingree, R.D., 1997. The principal lunar semidiurnal tide and its harmonics: baseline solutions for M2 and M4 constituents on the North-West European Continental Shelf. Continental Shelf Research 17 (11), 1321-1365, doi: 10.1016/S0278-4343(97)00007-1.

Slutz, R.J., Lubker, S.J., Hiscox, J.D., Woodruff, S.D., Jenne, R.L., Joseph, D.H., Steurer, P.M., Elms, J.D., 1985. Comprehensive Ocean-Atmosphere Data Set; Release 1. NOAA Environmental Research Laboratories, Climate Research Program, Boulder, CO, 268pp.

Song, Y.T., Haidvogel, D.B., 1994. A semi-implicit ocean circulation model using a generalized topography-following coordinate system. Journal of Computational Physics, 115 (1), 228-244.

Sotillo, M.G., Ratsimandresy, A.W., Carretero, J.C., Bentamy, A., Valero, F., Gonzalez-Rouco, F., 2005. A high-resolution 44-year atmospheric hindcast for the Mediterranean Basin: contribution to the regional improvement of global reanalysis. Climate Dynamics 25, 219-236, doi: 10.1007/s00382-005-0030-7.

Tomczak, M., Godfrey, J.S., 1994. Regional oceanography: An introduction. Pergamon, Oxford, 382pp.

Torrence, C., Compo, G.P., 1998. A Practical Guide to Wavelet Analysis. Bulletin of the American Meteorological Society 79, 61-78, doi: 10.1175/1520-0477(1998)079<0061:apgtwa>2.0.co;2.

Tsimplis, M.N., Woodworth, P.L., 1994. The global distribution of the seasonal sea level cycle calculated from coastal tide gauge data. Journal of Geophysical Research 99, 16031-16039, doi: 10.1029/94jc01115.

Valencia, V., Franco, J., Borja, A., Fontán, A., 2004. Hydrography of the southeastern Bay of Biscay. In: Borja, A. & Collins, M. (Eds.), Oceanography and Marine Environment of the Basque Country, Elsevier Oceanography Series, 70, 160-194.

van Aken, H.M., 2002. Surface currents in the Bay of Biscay as observed with drifters between 1995 and 1999. Deep-Sea Research Part I: Oceanographic Research Papers 49, 1071-1086, doi: 10.1016/S0967-0637(02)00017-1.

Vinogradov, S.V., Ponte, R.M., 2011. Low-frequency variability in coastal sea level from tide gauges and altimetry. J. Geophys. Res. 116, C07006, doi: 10.1029/2011jc007034.

Figures captions

Figure 1. Map of the Bay of Biscay showing the position of some geographical features mentioned in the text, such as Cape Ortegal, and the mouths of the Nervión, Adour and Gironde rivers. Solid black stars mark the position of the three tide gauge stations referred to in the text, namely, Bilbao, Boucau-Bayonne, and Port-Bloc. The 200, 500, 1000, 2000, 3000 and 4000 m isobaths from the ROMS bathymetry are shown for reference. The dashed gray line marks the limits of the model's domain.

Figure 2. (a) Time series of daily (3-day moving average) detrended atmospheric pressure (*MSLP*) at the closest point to the Bilbao tide gauge station; (b) time series of daily detrended sea level anomalies (*MSL*) for the Bilbao tide gauge station; (c) time series of daily (3-day moving average) detrended river discharge rates (*Q*) for the Nervión river; (d) same as in (b) but after applying the inverted barometer correction (*ASL*).

Figure 3. (a) Time series of daily (3-day moving average) detrended atmospheric pressure (*MSLP*) at the closest point to the Boucau-Bayonne tide gauge station; (b) time series of daily detrended sea level anomalies (*MSL*) for the Boucau-Bayonne tide gauge station; (c) time series of daily (3-day moving average) detrended river discharge rates (*Q*) for the Adour river; (d) same as in (b) but after applying the inverted barometer correction (*ASL*).

Figure 4. (a) Time series of daily (3-day moving average) detrended atmospheric pressure (*MSLP*) at the closest point to the Port-Bloc tide gauge station; (b) time series of daily detrended sea level anomalies (*MSL*) for the Port-Bloc tide gauge station; (c) time series of daily (3-day moving average) detrended river discharge rates (*Q*) for the Gironde; (d) same as in (b) but after applying the inverted barometer correction (*ASL*).

Figure 5. Cross wavelet power spectrum of *Q* and *MSL* for the Bilbao-Nervión system, displayed as a function of period and time. Colour contours represent cross wavelet power and vectors indicate the relative phase relationship between the two time series (with in-phase pointing right, anti-phase pointing left, *Q*/*MSL* leading *MSL*/*Q* by 90º pointing straight down/up). The wavelet power is normalized by $1/\sigma^2$, where σ^2 is the variance. The thin black line delineates the cone of influence (COI). The main periods discussed in the manuscript have been marked with black rectangles.

Figure 6. (a) Time series of daily (3-day moving average) detrended atmospheric pressure (*MSLP*) at the closest point to the Bilbao tide gauge station for year 2005; (b) time series of daily (3-day moving average) detrended river discharge rates (*Q*) for the Nervión river; (c) time series of pressure-adjusted sea level anomalies (*ASL*) for the Bilbao tide gauge station.

Figure 7. (a) Time series of daily (3-day moving average) detrended atmospheric pressure (*MSLP*) at the closest point to the Bilbao tide gauge station for year 1997; (b) time series of daily (3-day moving average) detrended river discharge rates (*Q*) for the Nervión river; (c) time series of pressure-adjusted sea level anomalies (*ASL*) for the Bilbao tide gauge station.

Figure 8. Cross wavelet power spectrum of *Q* and *MSL* for the Bayonne-Adour system, displayed as a function of period and time. Colour contours represent cross wavelet power and vectors indicate the relative phase relationship between the two time series (with in-phase pointing right, anti-phase pointing left, *Q*/*MSL* leading *MSL*/*Q* by 90º pointing straight down/up). The wavelet power is normalized by $1/\sigma^2$, where σ^2 is the variance. The thin black line delineates the cone of influence (COI).

Figure 9. (a) Time series of daily (3-day moving average) detrended atmospheric pressure (*MSLP*) at the closest point to the Boucau-Bayonne tide gauge station for year 2000; (b) time series of daily (3-day moving average) detrended river discharge rates (*Q*) for the Adour river; (c) time series of pressure-adjusted sea level anomalies (*ASL*) for the Boucau-Bayonne tide gauge station.

Figure 10. Cross wavelet power spectrum of *Q* and *MSL* for the Port-Bloc-Gironde system, displayed as a function of period and time. Colour contours represent cross wavelet power and vectors indicate the relative phase relationship between the two time

series (with in-phase pointing right, anti-phase pointing left, *Q*/*MSL* leading *MSL*/*Q* by 90º pointing straight down/up). The wavelet power is normalized by $1/\sigma^2$, where σ^2 is the variance. The thin black line delineates the cone of influence (COI).

Figure 11. (a) Time series of daily (3-day moving average) detrended atmospheric pressure (*MSLP*) at the closest point to the Port-Bloc tide gauge station for year 2004; (b) time series of daily (3-day moving average) detrended river discharge rates (*Q*) for the Gironde river; (c) time series of pressure-adjusted sea level anomalies (*ASL*) for the Port-Bloc tide gauge station.

Figure 12. Results obtained from the POT analysis for the (a) Bilbao - Nervión, (b) Bayonne-Adour, and (c) Port-Bloc - Gironde systems, respectively. Dots represent the extreme values obtained from the POT analysis and lines correspond to the regression fit performed. *ASL* values have been expressed in metres for plotting purposes.

Figure 13. ROMS results showing a region around the Nervión river. The 200 m isobath is shown for reference. Maps are calculated by subtracting, at each grid point, the sea level time series of the two model simulations under comparison and then computing the average value: (a) simulation with rivers (*R01*) versus *control run* for the full time period; (b) simulation with rivers and zero salinity (*R02*) versus *control run* for the full time period; (c) and (d) are equivalent to (a) and (b) but only for the extreme events as defined in the text.

Figure 14. ROMS results showing a region around the Adour river. The 200 m isobath is shown for reference. Maps are calculated by subtracting, at each grid point, the sea level time series of the two model simulations under comparison and then computing the average value: (a) simulation with rivers (*R01*) versus *control run* for the full time period; (b) simulation with rivers and zero salinity (*R02*) versus *control run* for the full time period; (c) and (d) are equivalent to (a) and (b) but only for the extreme events as defined in the text.

Figure 15. ROMS results showing a region around the Gironde river. The 200 m isobath is shown for reference. Maps are calculated by subtracting, at each grid point, the sea level time series of the two model simulations under comparison and then computing the average value: (a) simulation with rivers (*R01*) versus *control run* for the full time period; (b) simulation with rivers and zero salinity (*R02*) versus *control run* for the full time period; (c) and (d) are equivalent to (a) and (b) but only for the extreme events as defined in the text.

Figure 1

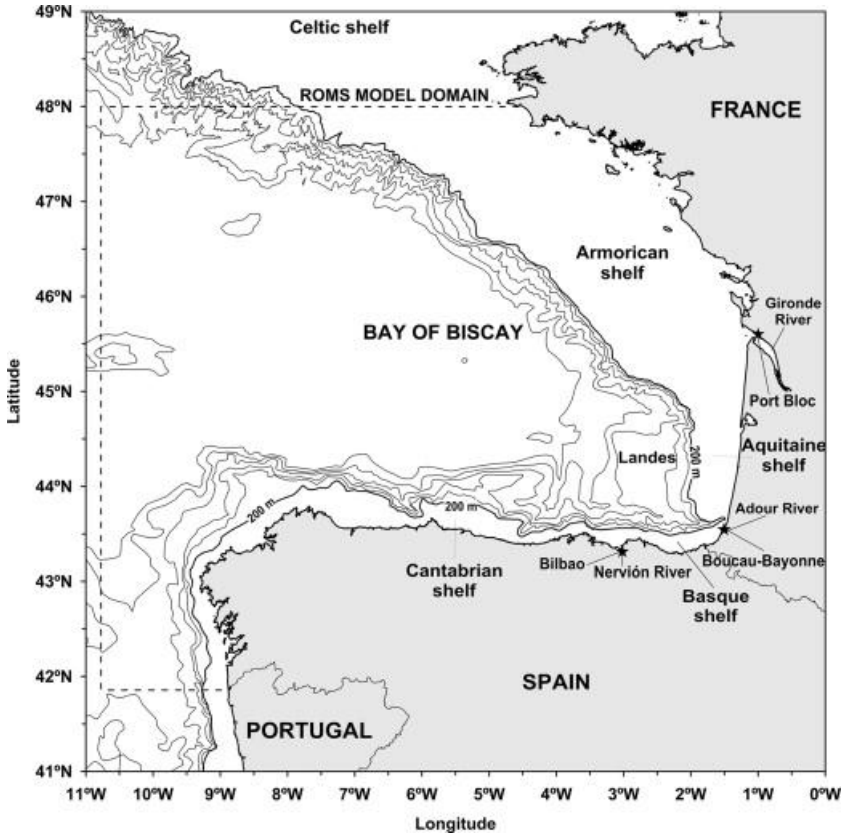

Figure 2

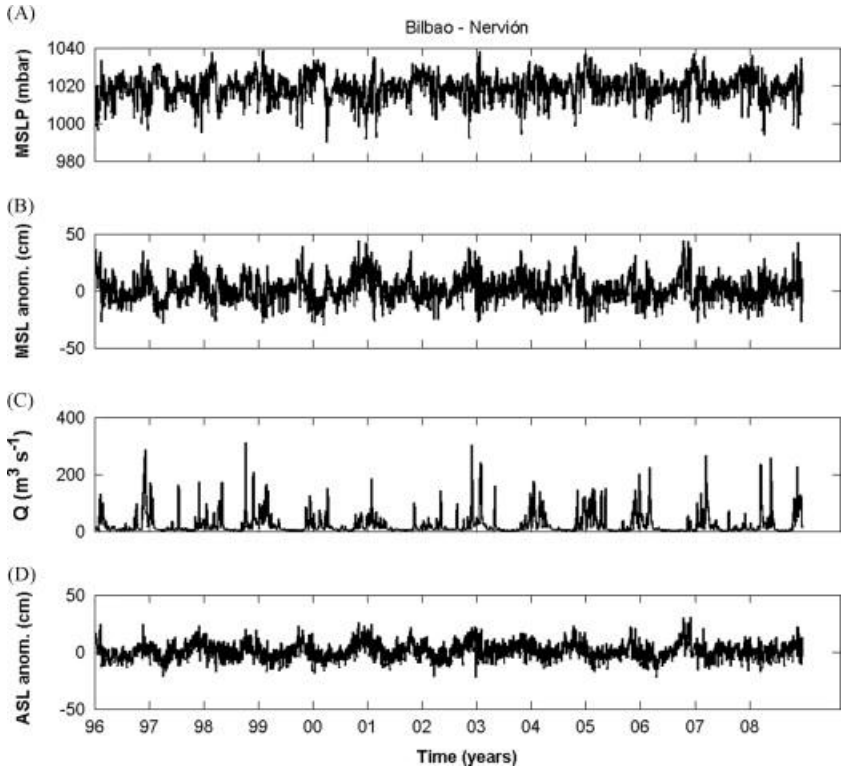

Figure 3

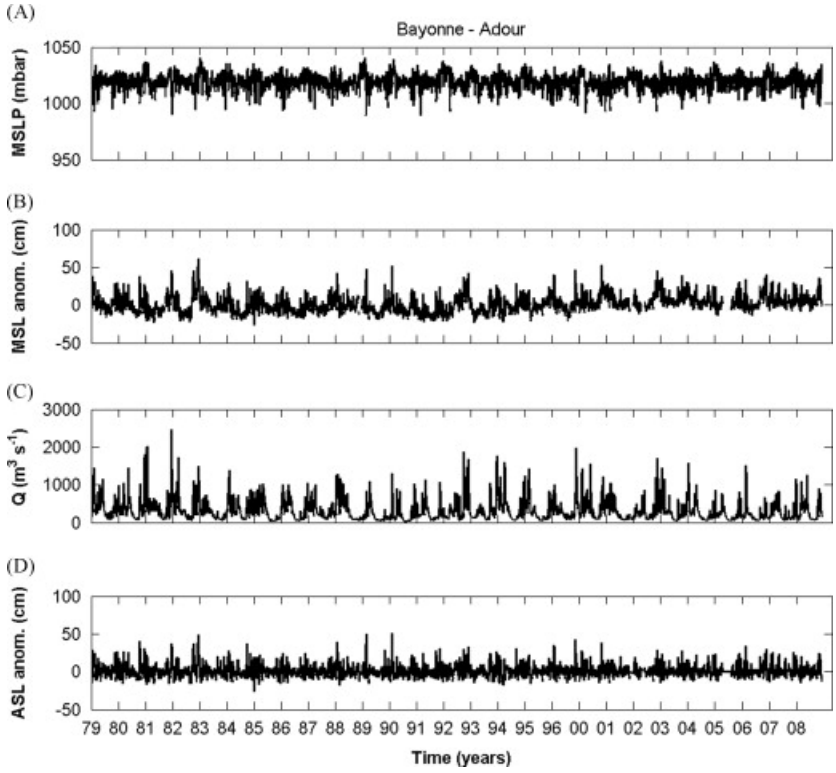

Figure 4

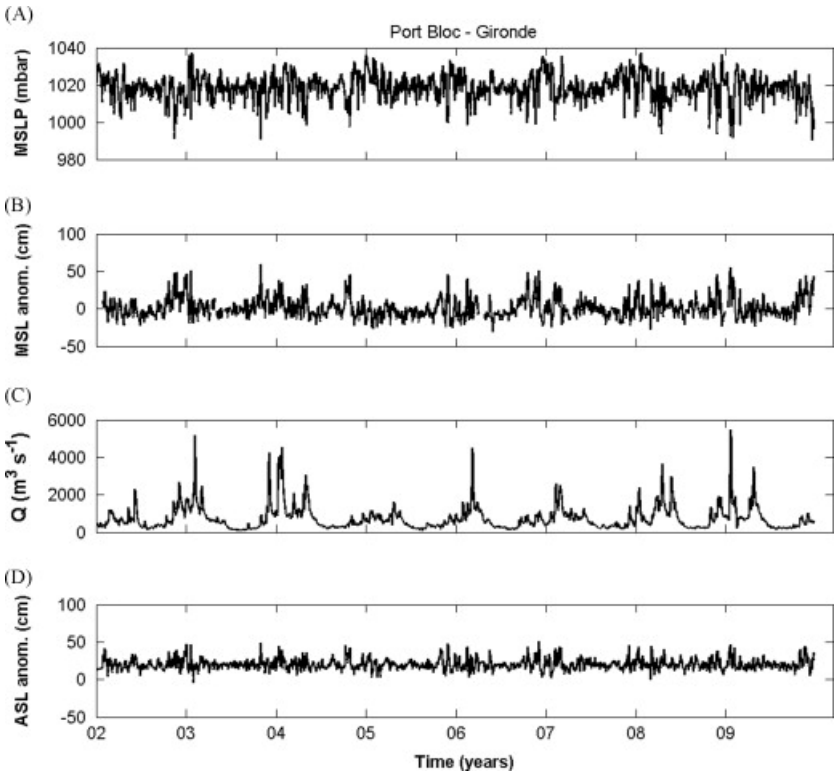

Figure 5

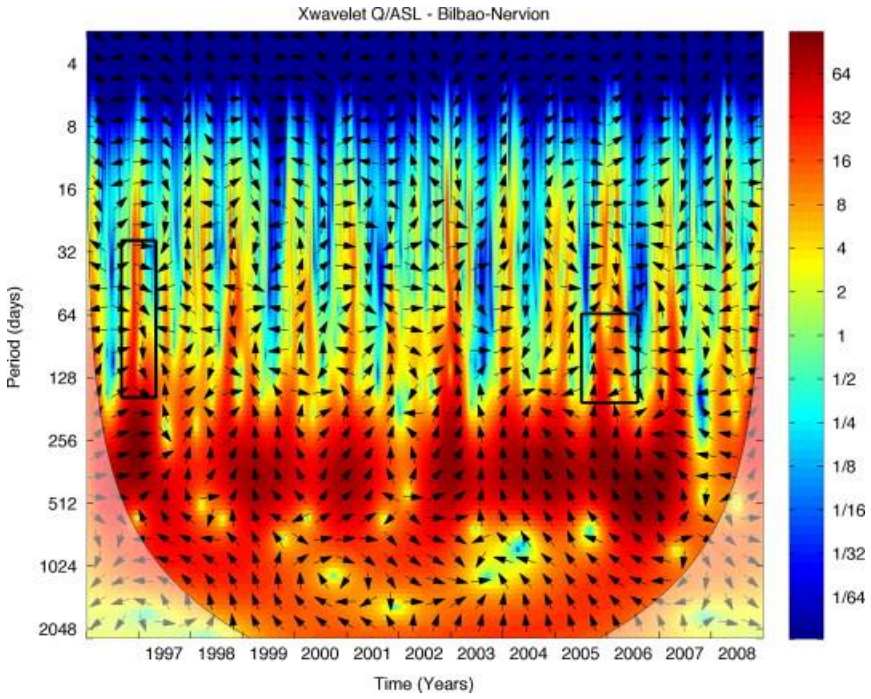

Figure 6

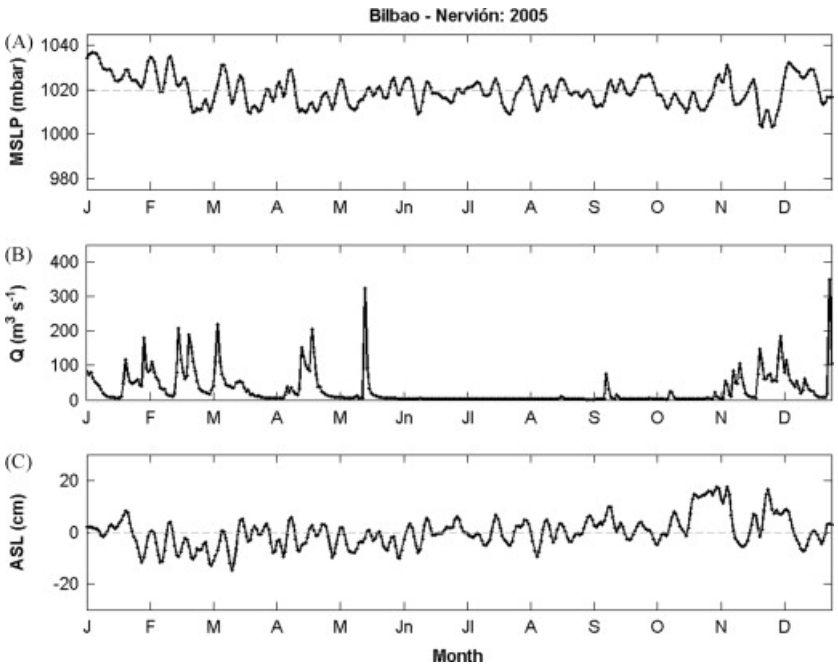

Figure 7

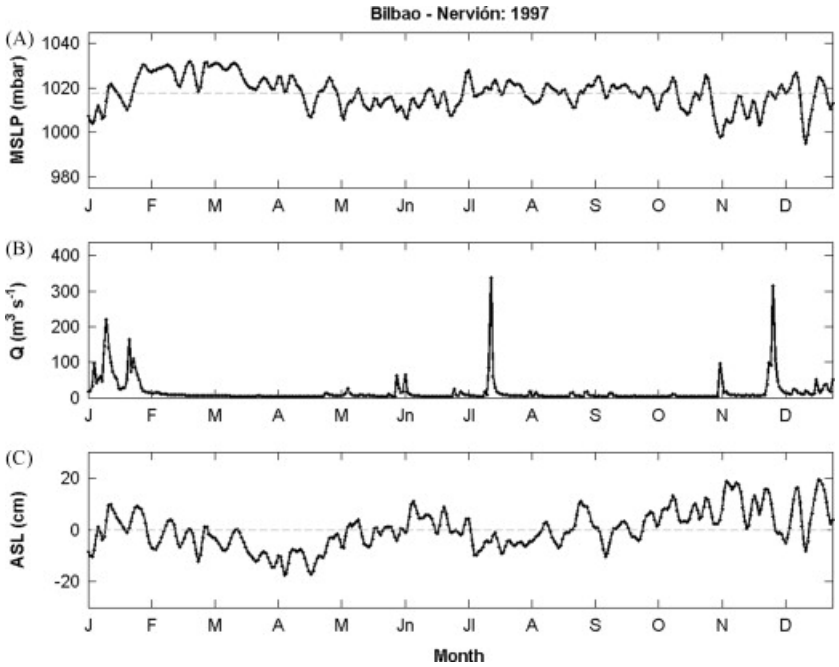
Bilbao - Nervión: 1997
(A)
MSLP (mbar)
1040
1020
1000
980
J F M A M Jn Jl A S O N D
(B)
Q (m3 s-1)
400
300
200
100
0
J F M A M Jn Jl A S O N D
(C)
ASL (cm)
20
0
-20
J F M A M Jn Jl A S O N D
Month

Figure 8

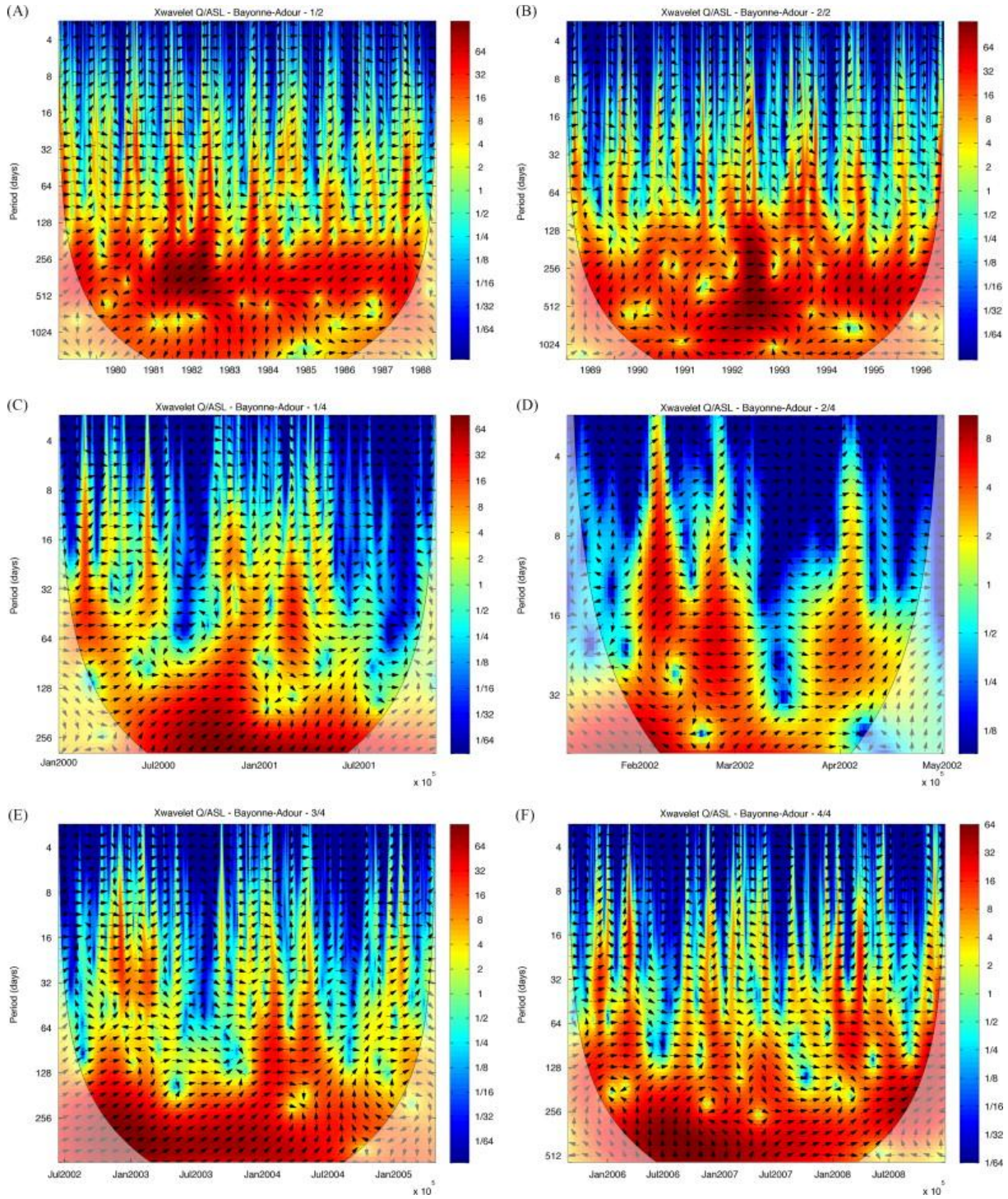
(A)
Xwavelet Q/ASL - Bayonne-Adour - 1/2
Period (days)
1980 1981 1982 1983 1984 1985 1986 1987 1988
(B)
Xwavelet Q/ASL - Bayonne-Adour - 2/2
Period (days)
1989 1990 1991 1992 1993 1994 1995 1996
(C)
Xwavelet Q/ASL - Bayonne-Adour - 1/4
Period (days)
Jan2000 Jul2000 Jan2001 Jul2001
x 10^5
(D)
Xwavelet Q/ASL - Bayonne-Adour - 2/4
Period (days)
Feb2002 Mar2002 Apr2002 May2002
x 10^5
(E)
Xwavelet Q/ASL - Bayonne-Adour - 3/4
Period (days)
Jul2002 Jan2003 Jul2003 Jan2004 Jul2004 Jan2005
x 10^5
(F)
Xwavelet Q/ASL - Bayonne-Adour - 4/4
Period (days)
Jan2006 Jul2006 Jan2007 Jul2007 Jan2008 Jul2008
x 10^5

Figure 9

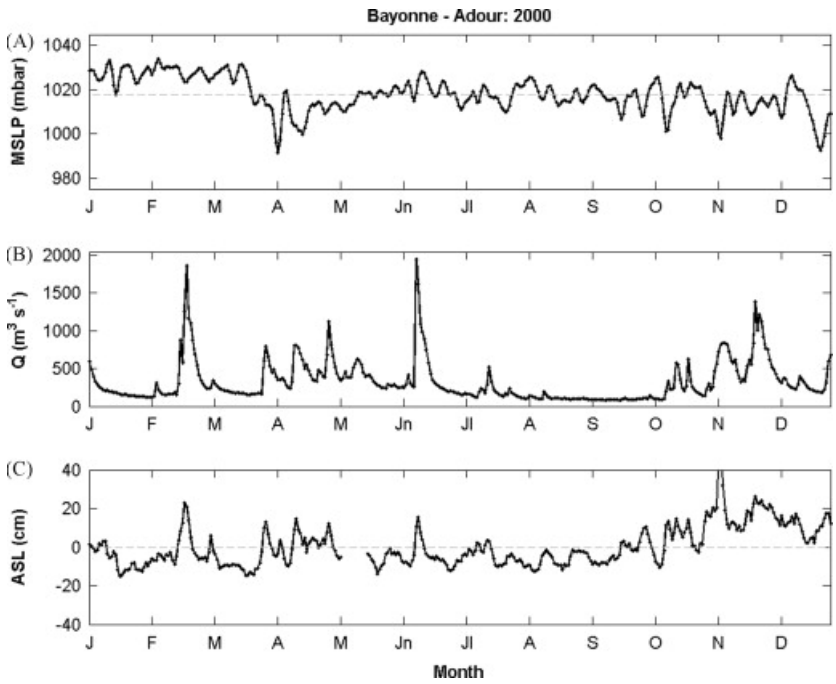

Figure 10

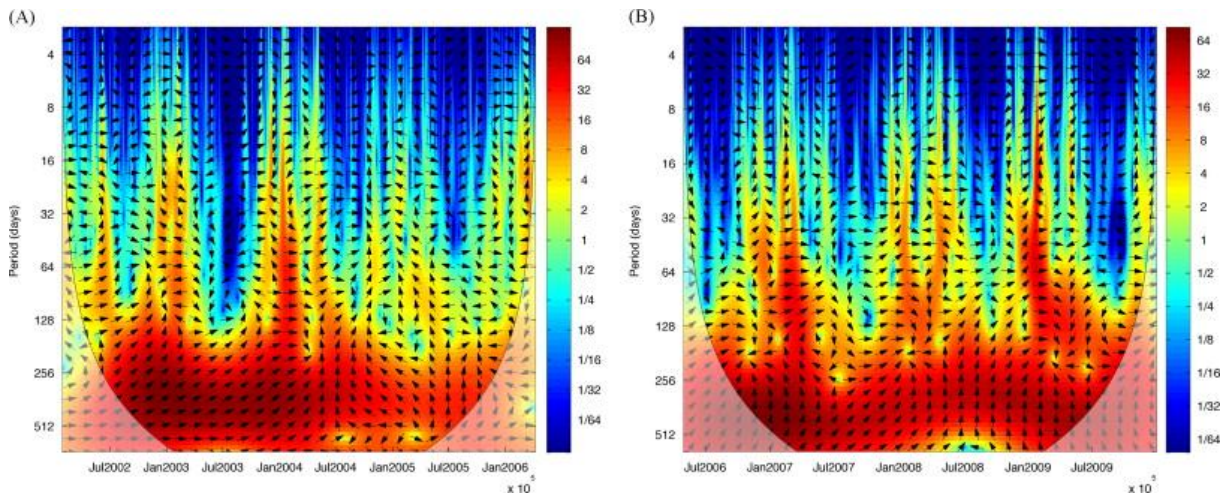

Figure 11

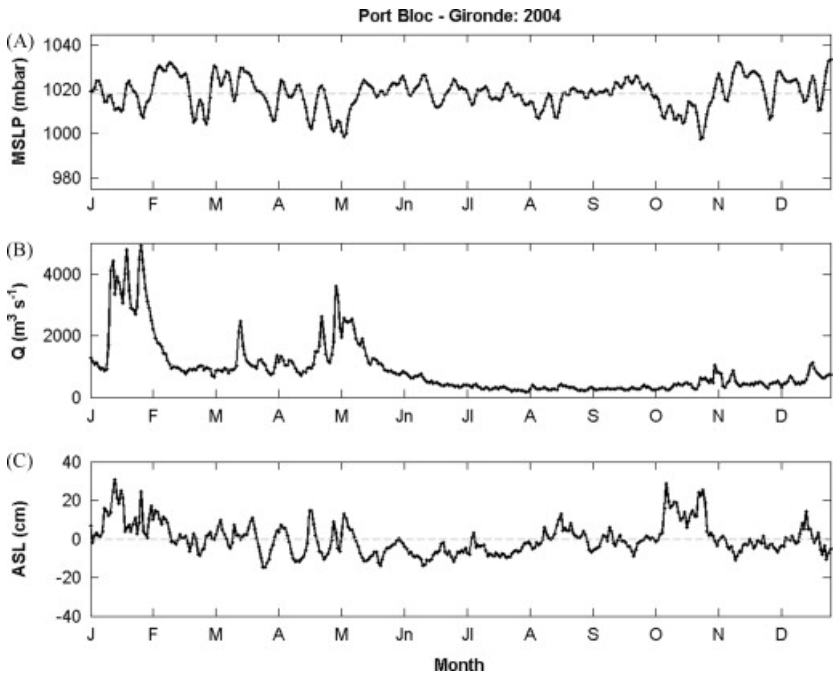

Figure 12

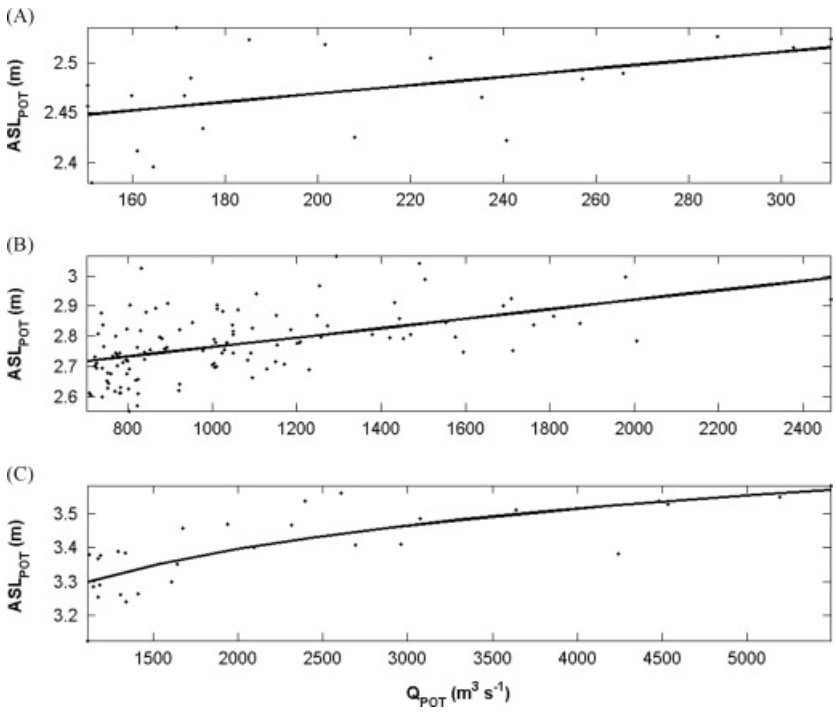

Figure 13

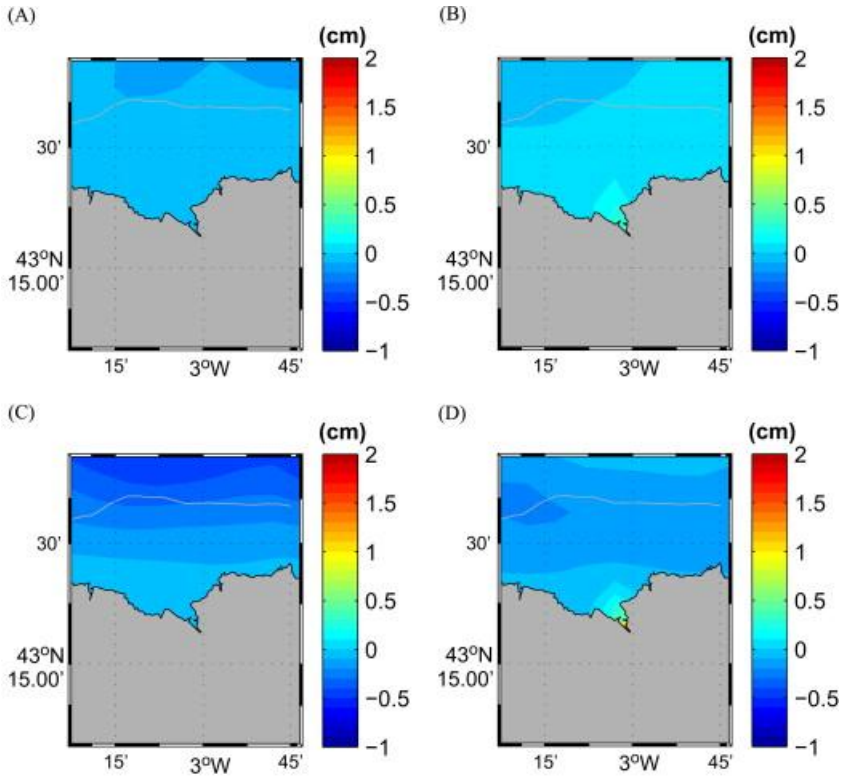

Figure 14

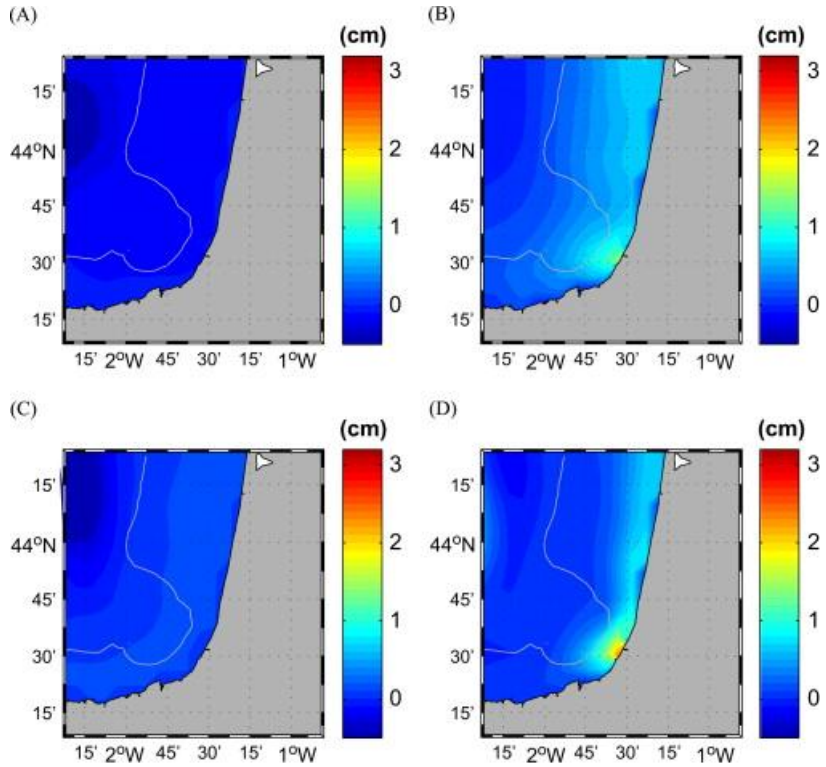

Figure 15